

AD-A101 856

COASTAL ENGINEERING RESEARCH CENTER FORT BELVOIR VA
LONGSHORE SAND TRANSPORT STUDY AT CHANNEL ISLANDS HARBOR, CALIF--ETC(U)
APR 81 R O BRUNO, R G DEAN, C G GABLE

F/6 13/2

UNCLASSIFIED

CERC-TP-81-2

NL

1 -
A101 856

END
DATE
8 81
OTIC

TP 81-2

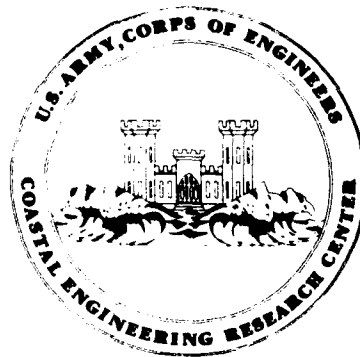
LEVEL II
12

ADA101856

Longshore Sand Transport Study
at
Channel Islands Harbor, California

by
R. O. Bruno, R. G. Dean,
C. G. Gable, and T. L. Walton, Jr.

TECHNICAL PAPER NO. 81-2
APRIL 1981



Approved for public release;
distribution unlimited.

DTIC ELECTE
S JUL 23 1981 D
D

U.S. ARMY, CORPS OF ENGINEERS
COASTAL ENGINEERING
RESEARCH CENTER

Kingman Building
Fort Belvoir, Va. 22060

81 7 22 052

DTIC FILE COPY
85

Reprint or republication of any of this material shall give appropriate credit to the U.S. Army Coastal Engineering Research Center.

Limited free distribution within the United States of single copies of this publication has been made by this Center. Additional copies are available from:

*National Technical Information Service
ATTN: Operations Division
5285 Port Royal Road
Springfield, Virginia 22161*

The findings in this report are not to be construed as an official Department of the Army position unless so designated by other authorized documents.

UNCLASSIFIED

SECURITY CLASSIFICATION OF THIS PAGE (When Data Entered)

REPORT DOCUMENTATION PAGE		READ INSTRUCTIONS BEFORE COMPLETING FORM
1. REPORT NUMBER TP-81-2	2. GOVT ACCESSION NO. <i>A D-A107 856</i>	3. RECIPIENT'S CATALOG NUMBER
4. TITLE (and Subtitle) LONGSHORE SAND TRANSPORT STUDY AT CHANNEL ISLANDS HARBOR, CALIFORNIA	5. TYPE OF REPORT & PERIOD COVERED Technical paper	9
7. AUTHOR(s) R.O. Bruno, R.G. Dean, C.G. Gable, and T.L. Walton, Jr.	6. PERFORMING ORG. REPORT NUMBER	
8. CONTRACT OR GRANT NUMBER(s)		
9. PERFORMING ORGANIZATION NAME AND ADDRESS Department of the Army Coastal Engineering Research Center (CEREN-FN) Kingman Building, Fort Belvoir, Virginia 22060	PROGRAM ELEMENT, PROJECT, TASK & WORK UNIT NUMBERS 31232	
11. CONTROLLING OFFICE NAME AND ADDRESS Department of the Army Coastal Engineering Research Center Kingman Building, Fort Belvoir, Virginia 22060	12. REPORT DATE <i>April 1981</i>	13. NUMBER OF PAGES 48
14. MONITORING AGENCY NAME & ADDRESS (if different from Controlling Office)	15. SECURITY CLASS. (of this report) UNCLASSIFIED	
	15a. DECLASSIFICATION/DOWNGRADING SCHEDULE	
16. DISTRIBUTION STATEMENT (of this Report) Approved for public release; distribution unlimited.		
17. DISTRIBUTION STATEMENT (of the abstract entered in Block 20, if different from Report)		
18. SUPPLEMENTARY NOTES		
19. KEY WORDS (Continue on reverse side if necessary and identify by block number) Channel Islands, California Littoral processes	Longshore energy flux Longshore sand transport	
20. ABSTRACT (Continue on reverse side if necessary and identify by block number) A field experiment was conducted to develop correlations between wave characteristics and longshore sediment transport. The waves were measured by two near-bottom mounted pressure transducers and by visual observation when pressure transducers were not in operation. The average longshore sediment transport rates were determined from sequential volumetric surveys behind an offshore breakwater which was regarded as a total trap. The data analyzed encompass a period of 2 years, 1 year after each dredging cycle.	(Continued)	

UNCLASSIFIED

SECURITY CLASSIFICATION OF THIS PAGE(When Data Entered)

Spectral analyses of the pressure gage wave data were conducted and yielded one direction per frequency. The correlations include immersed weight sediment transport rate, I , versus longshore component of wave energy flux at breaking, P_{LS} . The most widely used correlation constant, K , in the relationship $I = K P_{LS}$, is 0.77. The value determined from the data was $K = 0.98$, based on the P_{LS} values directed toward the trap. One feature of this type of trap is the potential for overtrapping if the waves are directed nearly normal to shore.

PREFACE

This report is published to provide coastal engineers with an updated method for prediction of sand transport along beaches (littoral drift). The prediction equation is calibrated with data from a 2-year study of longshore sand transport at Channel Islands Harbor, California. The work was carried out under the beach behavior and restoration program of the U.S. Army Coastal Engineering Research Center (CERC).

The report was prepared by R.O. Bruno, R.G. Dean, C.G. Gable, and T.L. Walton, Jr., under the general supervision of N.E. Parker, Chief, Engineering Development Division.

The authors acknowledge the assistance of the U.S. Army Engineer District, Los Angeles, and Dr. J.R. Weggel and D.W. Berg of CERC.

Comments on this publication are invited.

Approved for publication in accordance with Public Law 166, 79th Congress, approved 31 July 1945, as supplemented by Public Law 172, 88th Congress, approved 7 November 1963.


TED E. BISHOP
Colonel, Corps of Engineers
Commander and Director

Accession For	
NTIS GRA&I	<input checked="" type="checkbox"/>
DTIC TAB	<input type="checkbox"/>
Unannounced	<input type="checkbox"/>
Justification	
By _____	
Distribution/	
Availability Terms	
Avail and/or	
Dist	Specia
A	

CONTENTS

	Page
CONVERSION FACTORS, U.S. CUSTOMARY TO METRIC (SI)	6
SYMBOLS AND DEFINITIONS.	7
I INTRODUCTION	9
1. Purpose	9
2. Location and History.	9
3. Physiography and Littoral Processes	9
4. Past Longshore Sand Transport Relationships and Studies.	13
5. Discussion.	15
II DATA COLLECTION AND ANALYSIS	18
1. Bathymetric Survey Data Collection and Analysis	18
2. LEO Data Collection and Analysis.	24
3. Wave Gage Data Collection and Analysis.	29
4. Results of Longshore Sand Transport-Longshore Energy Flux Factor Correlation	36
5. Conclusions	38
LITERATURE CITED	40
 APPENDIX	
A DERIVATION OF EQUATION (9) FOR LONGSHORE ENERGY FLUX	43
B CALCULATIONS OF LONGSHORE ENERGY FLUX FACTORS.	45
 TABLES	
1 Summary of field data available for longshore transport correlation and characteristics of resulting K factor	16
2 Summary of survey data	19
3 Geometric characteristics of the two-gage array.	35
4 Shoreline orientation as determined from beach and offshore profiles	36
5 Summary of analyzed data	37
 FIGURES	
1 Channel Islands Harbor study area.	10
2 Wave sheltering at Channel Islands Harbor.	12
3 Comparison of field data with present SPM relationship	17
4 Plot of \bar{K} versus diameter, D.	17
5 Longshore sand transport study, Channel Islands, 1976-77	18

CONTENTS

FIGURES--Continued

	Page
6 Longshore transport study area	19
7 Illustrations of survey errors at reference station.	21
8 Fathometer record of regular bottom with waves and irregular bottom without waves.	21
9 Range 101+00 at beginning and end of study	22
10 Profile changes at range 109+00.	23
11 Elevation changes between 17 April and 30 July 1974 surveys.	23
12 Net longshore energy flux versus time for LEO stations 5714 and 5715	26
13 Comparison of observed wave heights (LEO) to recorded wave gage heights in phase I of study.	27
14 Comparison of observed wave heights (LEO) to recorded wave gage heights in phase II of study	28
15 Characteristics of a two-gage array at Channel Islands Harbor, California.	29
16 The two-gage array notation and directional ambiguity.	31
17 Sediment transport energy flux relationship for Channel Islands study	37
18 Summary of field data I versus P_{ls} , including results of this study.	38

CONVERSION FACTORS, U.S. CUSTOMARY TO METRIC (SI) UNITS OF MEASUREMENT

U.S. customary units of measurement used in this report can be converted to metric (SI) units as follows:

Multiply	by	To obtain
inches	25.4	millimeters
	2.54	centimeters
square inches	6.452	square centimeters
cubic inches	16.39	cubic centimeters
feet	30.48	centimeters
	0.3048	meters
square feet	0.0929	square meters
cubic feet	0.0283	cubic meters
yards	0.9144	meters
square yards	0.836	square meters
cubic yards	0.7646	cubic meters
miles	1.6093	kilometers
square miles	259.0	hectares
knots	1.852	kilometers per hour
acres	0.4047	hectares
foot-pounds	1.3558	newton meters
millibars	1.0197×10^{-3}	kilograms per square centimeter
ounces	28.35	grams
pounds	453.6	grams
	0.4536	kilograms
ton, long	1.0160	metric tons
ton, short	0.9072	metric tons
degrees (angle)	0.01745	radians
Fahrenheit degrees	5/9	Celsius degrees or Kelvins ¹

¹ To obtain Celsius (C) temperature readings from Fahrenheit (F) readings, use formula: $C = (5/9)(F - 32)$.

To obtain Kelvin (K) readings, use formula: $K = (5/9)(F - 32) + 273.15$.

SYMBOLS AND DEFINITIONS

$a_1, a_p, a_\eta;$	Fourier coefficient for signal 1, pressure signal, and water surface elevation signal
b_1, b_p, b_η	
C	wave celerity at breaking depth
c_f	friction coefficient
c_{12}	cospectra of signals 1 and 2
D	sediment size
d	water depth
d_b	water depth at breaking
E	energy density of waves (below spacial aliasing frequency)
E_{TOT}	total energy density
F	modulus of wave amplitude spectrum
F_R	onshore energy flux at gage location
F_b	onshore energy flux at breaking
G	ratio of total energy to energy below spacial aliasing frequency
g	acceleration of gravity
H_b	breaking wave height
H_{rms}	root-mean-square wave height
H_{rms_b}	root-mean-square wave height at breaking
H_s	significant wave height
I	immersed weight sediment transport rate
i	index number
j	index number
K	dimensionless constant relating sand transport to longshore energy flux
K^*	dimensional constant relating sand transport to longshore energy flux
K_p	pressure response factor

SYMBOLS AND DEFINITIONS--Continued

k_n	wave number at frequency index n
L	wavelength
ℓ	pressure gage spacing
N	number of time series points
n	index number
P	dimensionless mixing parameter
P_{ls}	longshore energy flux
P_1, P_2	pressure signals, 1 and 2
P'_1, P'_2	data window modified pressure signals 1 and 2
p	porosity of sediment
q_{12}	quad-spectra of signals 1 and 2
S_G	distance of pressure sensors above bottom
S_{12}	auto spectrum of signals 1 and 2
v	longshore velocity
v_o	longshore velocity at breaking (no mixing)
w	width of surf zone
w	data window weighting factor
α	wave angle with shoreline
α_b	wave angle with shoreline at breaking
β	angle of gage axis with shore normal
γ	specific weight of water
Δd	water depth over pressure sensors
ϵ	phase lag
η	water surface elevation from mean water surface
$\overline{\eta^2}$	mean square water surface elevation
κ	ratio of breaking wave height to depth
π	3.14159
ρ	mass density of water
ρ_s	mass density of sediment
σ	circular wave frequency
σ_K	standard deviation of K's

LONGSHORE SAND TRANSPORT STUDY AT CHANNEL
ISLANDS HARBOR, CALIFORNIA

by
R.O. Bruno, R.G. Dean, C.G. Gable, and T.L. Walton, Jr.

I. INTRODUCTION

1. Purpose.

The relationship between longshore sand transport in the surf zone and wave energy is of vital interest to coastal engineers concerned with design and maintenance of navigation and beach erosion control projects. As discussed in the Shore Protection Manual (SPM) (U.S. Army, Corps of Engineers, Coastal Engineering Research Center, 1977), past field and laboratory studies have produced a widely used empirical relationship for sand transport in a shore-parallel direction; however, these studies were conducted in areas where total transport may not have been measured. In this study, Channel Islands Harbor, California (Fig. 1), was selected for measuring longshore sand transport because an offshore breakwater and twin jetties at the site form a unique sand trap. This site is considered to be nearly a total littoral barrier to longshore sand transport moving in a southerly direction (Herron and Harris, 1966). A further advantage to the Channel Islands site is its exposure to high wave energy climate with a dominant wave direction out of the west and northwest and consequently, high sand transport rates in a predominantly southerly direction along the beaches. Dredging records from the harbor show annual transport in excess of 1 million cubic meters (Herron and Harris, 1966). The objective of this study was to obtain additional data on longshore sand transport in order to reevaluate the present semiempirical relationship for longshore sand transport given in Chapter 4 of the SPM.

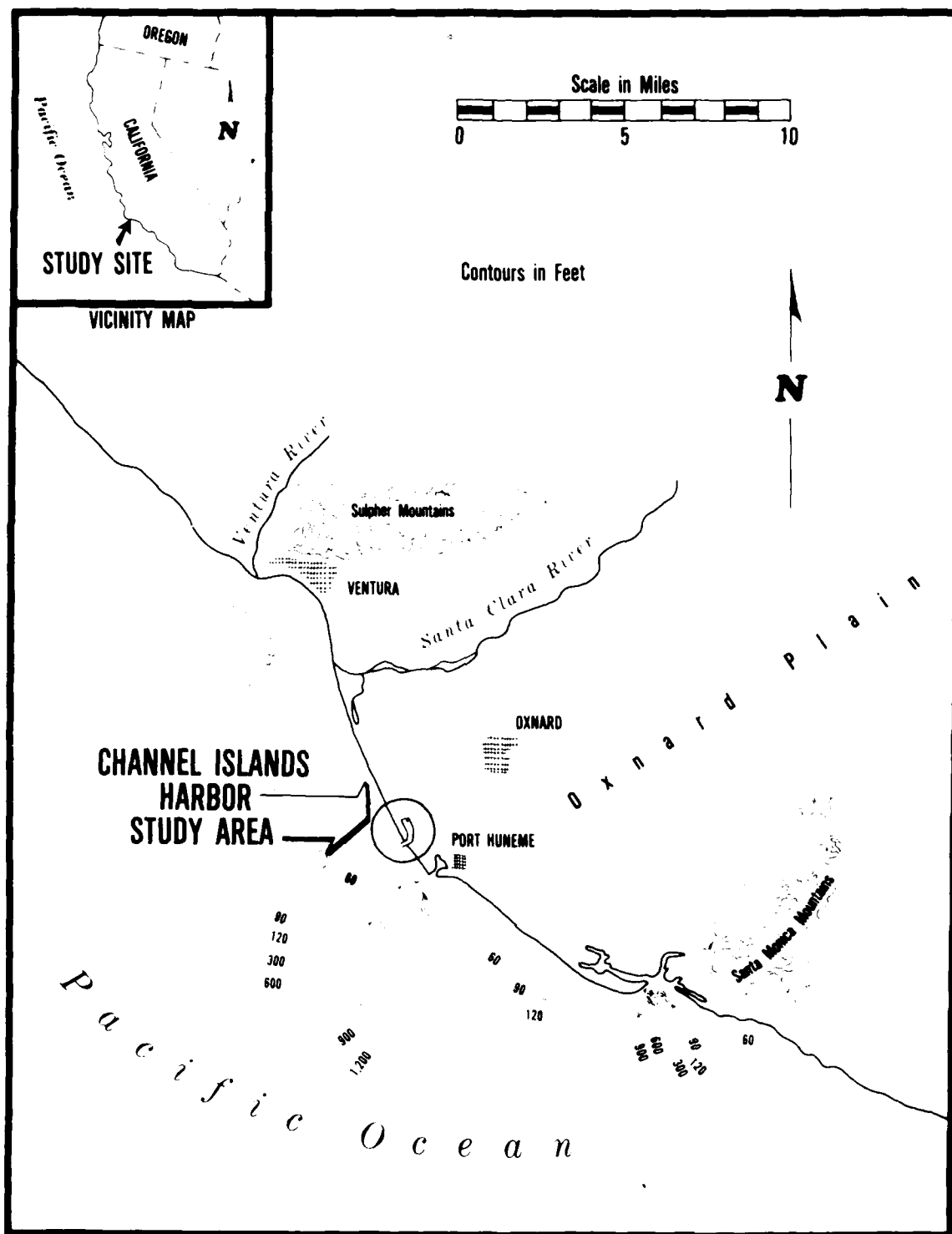
2. Location and History.

Channel Islands Harbor is located about 110 kilometers northwest of Los Angeles and 1.6 kilometers upcoast (northwest) of Port Hueneme (Fig. 1). The harbor consists of entrance jetties and an offshore breakwater which were constructed to provide a solution to a downcoast beach erosion problem and to provide a small-craft harbor. Before the harbor construction, a serious erosion problem existed downcoast (southeast) of Port Hueneme which has been attributed to diversion of littoral sands into the Hueneme Canyon by the Port Hueneme north jetty. Presently, sand trapped at Channel Islands Harbor is bypassed to the south of Port Hueneme by periodic dredging (U.S. Army Engineer District, Los Angeles, 1948; Herron and Harris, 1966).

The offshore breakwater is 700 meters long, is located 600 meters offshore in a water depth of 9 meters, and trends roughly parallel to the shore. The design of the sand trap was developed empirically by considering the configuration of the Santa Monica, California, breakwater fillet and by developing diffraction patterns for generally prevailing waves (U.S. Army Engineer District, Los Angeles, 1948; Herron and Harris, 1966).

3. Physiography and Littoral Processes.

The shoreline at the site forms the coastal edge of the Oxnard Plain, an abandoned flood plain of the Santa Clara River (Fig. 1). The low, flat flood



plain extends about 21 kilometers along the shoreline and 13 kilometers inland, and is bounded on the north by the Sulphur Mountains and on the south by the Santa Monica Mountains. These mountains terminate at the sea in hard, wave-resistant formations, forming the south bank of the Ventura River and Point Mugu, respectively. The principal drainage features are the Ventura and Santa Clara Rivers. Offshore slopes in this area are gentle except where the steep-walled Hueneme and Mugu submarine canyons cut the Continental Shelf to within 0.4 kilometer of the shore.

Figure 2 is a view of the study area in relation to offshore islands and shows that much of the wave action is intercepted or modified by Point Conception or the offshore islands. The principal avenues of wave approach are from the same direction, hence, sea and swell arrive predominantly from the northwest and west. Local winter storms of short duration and a limited amount of summer swell, originating from the south Pacific Ocean, reach the Hueneme area from the southwest and create short periods of northward littoral drift. However, wave studies and long observation of the shoreline processes show conclusively that there is a great preponderance of southward littoral drift (Herron and Harris, 1966).

There is one source area of littoral material, in addition to updrift beaches, for the Channel Islands study site (Fig. 1)--the Santa Clara River which discharges at the upper end of the Oxnard Plain. At irregular intervals of 10 to 30 years, tremendous floodflows occur that form a large delta at the mouth of the river extending as much as 0.8 kilometer seaward of the normal alignment of the shore (Herron and Harris, 1966). However, there is no accurate measure of the rate at which littoral material is supplied by the river.

At Port Hueneme, the Hueneme submarine canyon extends to within about 300 meters of the shore and is the one major sink for littoral materials in the Channel Islands area. The profile from mean lower low water (MLLW) to the -18-meter depth steepens from a normal of 1 on 100 to 1 on 4 into the canyon. The steep slopes of this canyon continue to depths as great as 1.5 kilometers.

Past estimates of littoral sand transport have shown a net southward sand transport on the order of 920,000 cubic meters per year for the beach area between the Hueneme and Mugu submarine canyons, based on shoreline erosion surveys before the Channel Islands bypassing operation (Herron and Harris, 1966).

The entrance to Channel Islands Harbor was dredged in 1960-61, and since that time the material impounded in the sediment trap has averaged approximately 1 million cubic meters per year; the capacity of the trap is approximately 2 million cubic meters. The material is usually pumped (on a biennial basis) a distance of about 2 kilometers to the downdrift side of the entrance to Port Hueneme, although material is occasionally placed in the "pocket beach" formed by the southeastern jetty to Channel Islands Harbor and the northwestern jetty to the Port Hueneme entrance approximately 1.6 kilometers to the southeast (Herron and Harris, 1966).

The net sediment transport is from northwest to southeast, but periods of reversal do occur. The average sediment size at the site is approximately 0.20 millimeter, the textural characteristics of the material deposited in the trap were reported in Bruno, Watts, and Gable (1977).

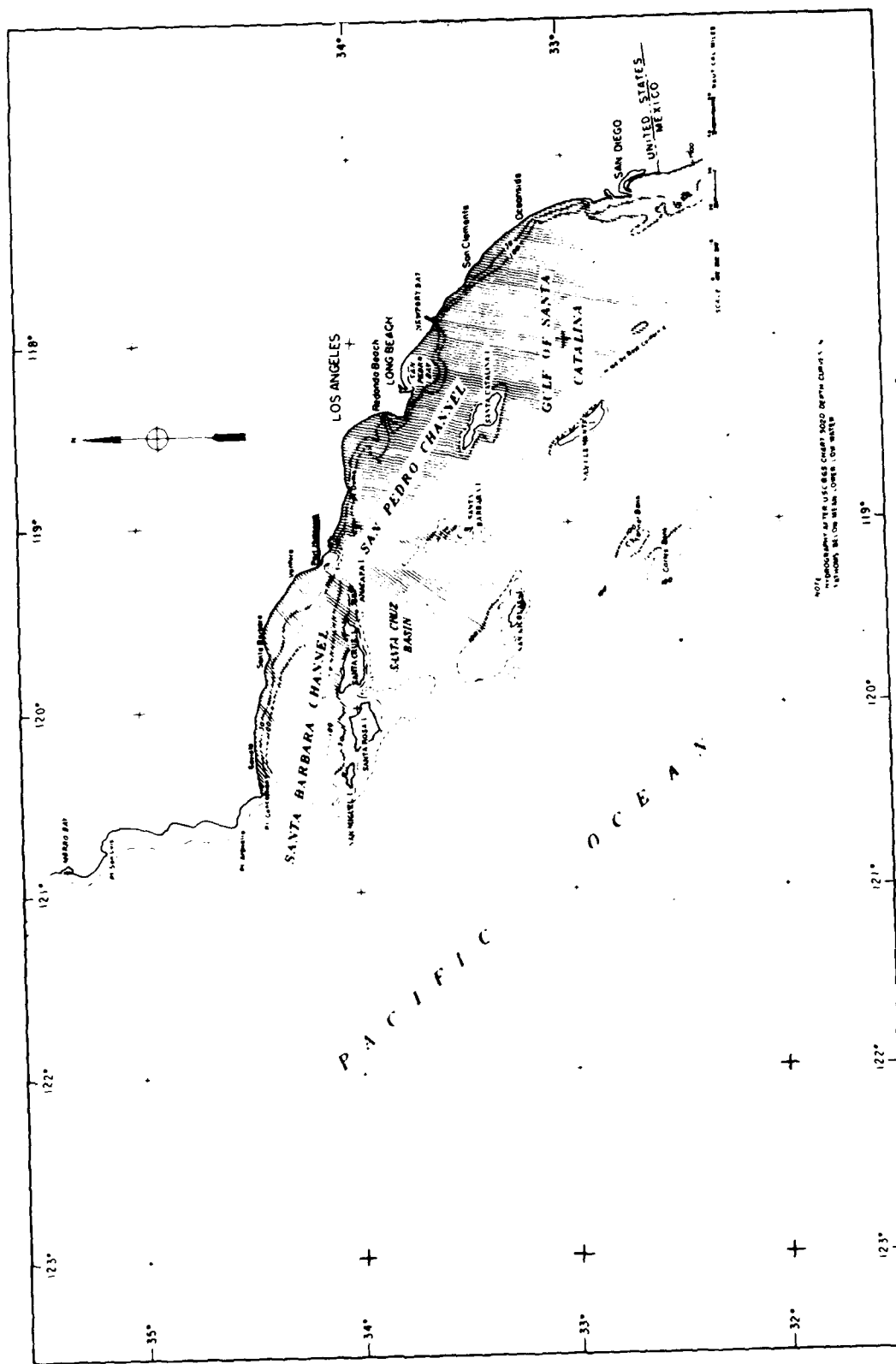


Figure 2. Wave sheltering at Channel Islands Harbor.

One feature of an offshore breakwater is that it tends to "overtrap" material, especially when waves approach in a direction nearly perpendicular to the shoreline. This effect can be demonstrated by noting that even for waves propagating directly toward shore, the effects of diffraction will cause deposition in the form of a salient or tombolo behind the breakwater. If this deposited material is removed such that an equilibrium topography does not exist, more material will be transported behind the breakwater, etc. Unfortunately, the degree of overtrapping for different wave characteristics is currently unknown. A related question of whether the impounded volumes should be correlated with the net or downdrift component of longshore energy flux is discussed in Section II.

For more detailed analyses of shoreline changes and historical bypassing operations in this area, see Beach Erosion Board (1953), Savage (1957), and Herron and Harris (1966).

4. Past Longshore Sand Transport Relationships and Studies.

The relationship between immersed weight transport rate of sediment, I , and longshore energy flux factor at breaking, P_{ls} , is generally presented in terms of a dimensionless constant, K (e.g., Vitale, 1980).

$$I = K P_{ls} \quad (1)$$

where for a single wave train of breaking height, H_b , and breaking direction, α_b , relative to a normal to the beach, P_{ls} can be expressed as

$$P_{ls} = \frac{\gamma H_b^2}{8} C \sin \alpha_b \cos \alpha_b \quad (2)$$

in which γ is specific weight of water, and C the wave group speed at breaking. A more useful form of equation (1) is obtained by noting that the immersed weight transport rate, I , and bulk longshore sediment transport, Q , are related by

$$Q = \frac{I}{\rho \left(\frac{\rho_s}{\rho} - 1 \right) g (1 - p)} \quad (3)$$

in which ρ and ρ_s are the mass densities of water and sediment, respectively, g the gravitational constant, and p the inplace porosity of the sediment. Combining equations (1) and (3)

$$Q = \frac{K}{\rho \left(\frac{\rho_s}{\rho} - 1 \right) g (1 - p)} P_{ls} = K^* P_{ls} \quad (4)$$

The above equations for longshore sediment transport do not account for sediment size, beach slope, porosity, etc.; therefore, it is very unlikely that K is a true constant. Tests conducted to date have not provided the ranges of independent variables (e.g., sediment size) or accuracy necessary to distinguish the effects of these variables, although models which account for the effects of these variables have been postulated (Dean, 1973; Walton, 1979).

The right side of equation (4) is the manner in which the sand transport relationship is presented in the SPM, where K^* is assumed constant and has dimensional units.

Available field data indicate that none of the approximately 56 data points are based on both measured wave direction and volumetric accumulations in a total trap. Some are based on visually observed wave directions at a location quite distant from the measured wave heights. In addition, much of the sediment data are based on tracer studies with the attendant uncertainties in estimating depth of effective motion.

The following brief review of field data on sand transport relationships, used in the SPM and other studies (see Galvin and Schweppe, 1980), is helpful in assessing the currently used relationship. Laboratory data have been omitted as they do not represent a properly scaled version of the prototype, since the scaled sediment size is significantly larger than is usually present with sand-sized particles. The review is presented in chronological order of the various investigations which yielded the data. Other reviews include Das (1971) Greer and Madsen (1978), and Bruno, Dean, and Gable (1980).

a. South Lake Worth Inlet, Florida (Watts, 1953). Longshore transport rates were based on quantities of sand transferred by a permanent sand bypassing plant on the north jetty of South Lake Worth Inlet. The pressure drop of the bypassing pump was correlated with sand discharge by a series of pumping events into a diked disposal area on the downdrift (south) side of the inlet and subsequent surveys of the associated volumes. Thereafter, transport rates were inferred from the (calibrated) pressure drop of the pump. Wave characteristics were based on (1) wave height measurements from a staff gage mounted on the South Lake Worth pier about 16 kilometers north of the inlet, and (2) visual observations of wave direction at the surfline as obtained from a vantage point about 6 kilometers north of the inlet. This study yielded four data points with a sediment diameter of approximately 0.4 millimeter. The average K value is 0.90 with a standard deviation of 0.11.

b. Anaheim Bay, California (Caldwell, 1956). Dredged material from the entrance to Anaheim Bay was placed on the downdrift (southeast) shore, and repeated surveys of this area were conducted as the material was transported in a southerly direction. Changes in volume were interpreted as longshore transport rates and estimates of longshore component of wave energy flux were based on (a) wave staff measurements from the Huntington Beach pier about 9 kilometers to the south, and (b) wave directions based on hindcasts and recognition of the sheltering by the offshore islands for waves originating from certain directions. This study provided five data points with a sediment diameter of approximately 0.40 millimeter. The average K value is 0.76 with a standard deviation 0.38.

c. Cape Thompson, Alaska (Moore and Cole, 1960). The growth of a spit and associated waves were observed over a 3-hour period. Spit volumes were measured by plane table survey, and wave characteristics were based on visual estimates. Only one data point was obtained with a K value of 0.25 for a sediment diameter of 1.00 millimeter.

d. Silver Strand, California, and El Moreno, Baja California (Komar and Inman, 1970). These data represent transport over fairly short-time intervals as determined from sand tracer measurements and wave energy fluxes derived

from an array of wave sensors. Sand transport volumes were usually determined over a fraction of a tidal cycle as the product of the width of the surf zone, the longshore displacement of the center of gravity of the tracer, and the thickness of tracer movement. The latter quantity was based on observations of the depth to which a cylindrical "plug" of tracer had eroded over the observational period and depth of tracer in cores; depth values ranged between 2 and 10.5 centimeters. These measurements yielded a total of 14 data points, and the average and standard deviation values of K for Silver Strand (4 data points) are 0.77 and 0.18, respectively; the average sediment size was 0.18 millimeter. These values for El Moreno (10 data points) are 0.82 and 0.27, respectively; the average sediment size was 0.60 millimeter.

e. Channel Islands Harbor, California (Bruno and Gable, 1976). Data in this report were based on the same general field program that is the subject of the present report. Sediment transport rates were inferred from volumetric accumulations behind the Channel Islands Harbor offshore breakwater, and the longshore energy flux values were based on Littoral Environmental Observations (LEO). A total of 13 data points resulted with average K and standard deviation values of 1.61 and 1.19, respectively. Sediment size was approximately 0.2 millimeter. These data were not used in the SPM sand transport relationship.

5. Discussion.

The results presented above comprise a total of 37 data points which, excluding Bruno and Gable's (1976) data, are summarized in Table 1 and presented in Figure 3. Figure 3 represents the SPM sand transport relationship in the dimensionless form of the equation. Figure 4 attempts to discern any effect of sediment size D on the quantity K . There is a fairly reasonable relationship of increasing K with decreasing sediment size, although there is only one data point for a sediment size exceeding 0.6 millimeter.

In general, it appears that none of the data sets provide the confidence that should be associated with both the wave and sediment volume data. In those studies with well-established volumetric data, the wave data usually included one or more visually estimated wave parameters (height and direction). In the reported tracer studies, it is believed that the inferred sediment transport rates overestimate the actual transport. This expected bias is probably due to the estimate of the shore-parallel displacement of the center of gravity of tracer displacement being obtained from the upper 5 centimeters of the sediment column, since shear transport must exist within the sand bed with the upper layers moving most rapidly. Additionally, the use of a single value of transport thickness based on the erosion depth of a tracer plug should increase bias as the maximum erosion depth is expected to increase with time. Finally, the longshore sediment transport in the surf zone is expected to be both spatially and temporally variable although these scales are currently unknown. Since the tracer studies represent longshore sediment transport over only a part of a tidal cycle, it is surprising that the studies do not exhibit greater scatter, i.e., standard deviations of 23 and 33 percent for the Silver Strand and El Moreno K values, respectively. One advantage of a relatively long-term, complete sediment trap is that it integrates the temporal and spatial variability, thereby providing a good basis for investigating the mean structure of the transport phenomenon before attempting to measure and understand the fine structure.

Table 1. Summary of field data available for longshore transport correlation and characteristics of resulting K factor.¹

Investigator	Location	Sediment diameter D (mm)	Data points (No.)	Transport	Waves ² height	Direction	Characteristics of K		
							Methods	R	σ_K
Watts (1953)	South Lake Worth Inlet, Fla.	0.40	4	Calibrated bypassing pump	M	0	0.90	0.11	19
Caldwell (1956)	Anaheim, Calif.	0.40	5	Surveys	N, H	H	0.76	0.38	50
Moore and Cole (1960)	Cape Thompson, Alaska	1.00	1	Measured spit growth	O	O	0.25	--	--
Kemar and Inman (1970)	Silver Strand, Calif.	0.18	4	Tracers	M	N	0.77	0.18	23
Komar and Inman (1970)	El Moreno, Baja Calif.	0.60	10	Tracers	M	N	0.82	0.27	33
Bruno and Gable (1976)	Channel Islands Harbor, Calif.	0.20	13	Offshore breakwater trap	O	O	1.61	1.19	74

¹I = KP_{ls} , I = immersed weight transport rate, P_{ls} = longshore energy flux of waves.

²M = Measured, O = observed, H = hindcast.

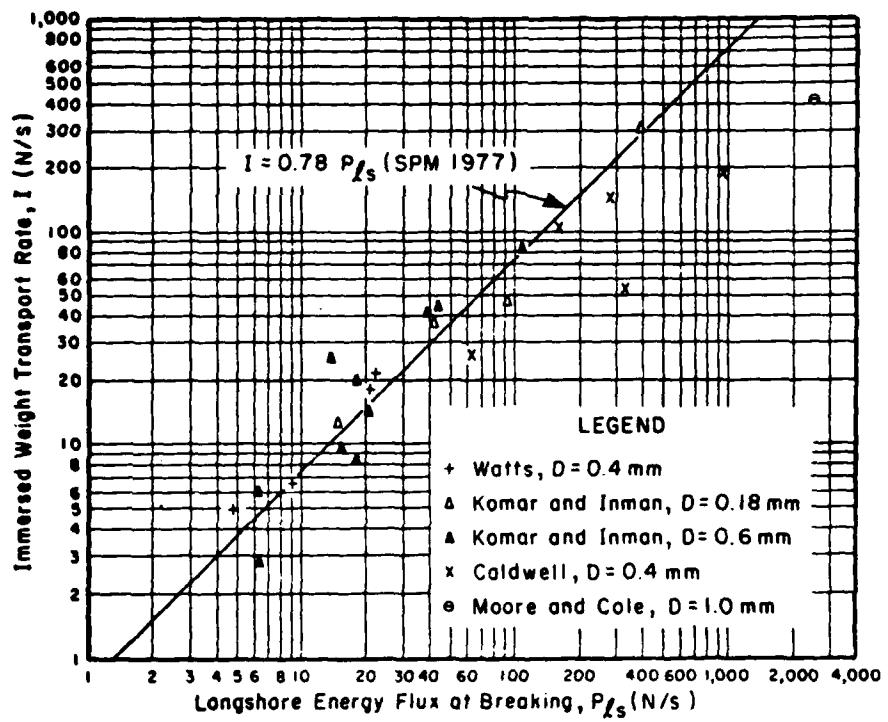


Figure 3. Comparison of field data with present SPM relationship.

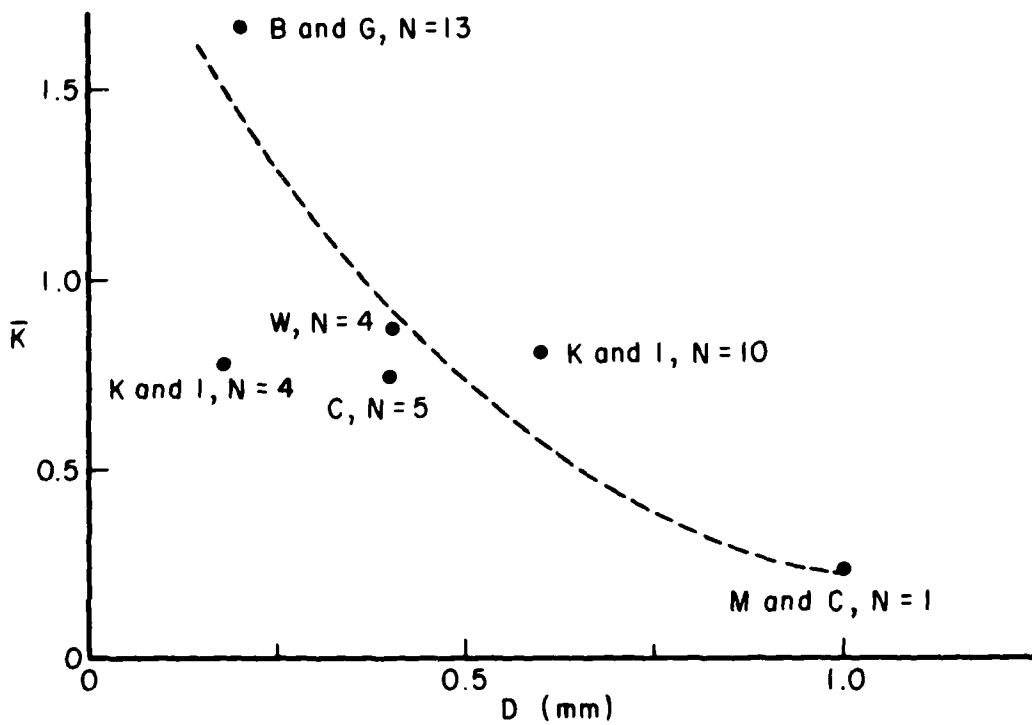


Figure 4. Plot of \bar{K} versus diameter, D . Initials and numbers, N , refer to investigators and number of data points comprising K .

The complexity of longshore sediment transport, the uncertainties and differences exhibited in available data, and the economic and functional impact of a valid quantitative predictor of transport certainly justify substantial future field and laboratory investigations.

II. DATA COLLECTION AND ANALYSIS

The data collection program consisted of periodic bathymetric and topographic surveys, routine wave data from which longshore transport and the wave energy flux could be calculated, and sediment samples taken during the study period to obtain quantitative information on the sand size at the site. Much of the information used here was reported in Bruno and Gable (1976).

The wave data included both LEO (Berg, 1968; Bruno and Hiipakka, 1972) and gage data from two wave pressure sensors installed at the site. A chart describing the various types of data collected and the survey dates from 1974 to 1977 is presented as Figure 5.

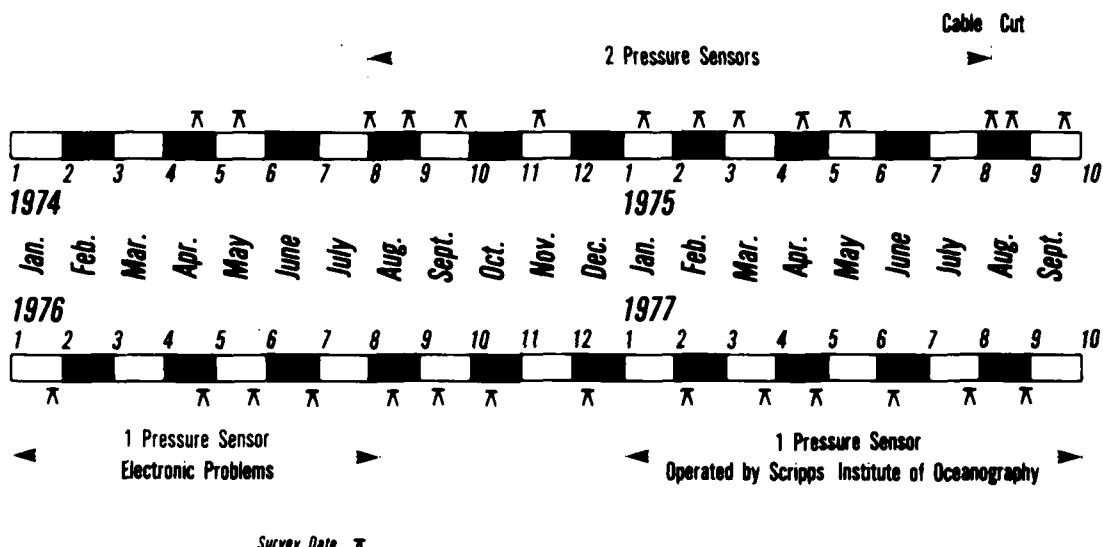
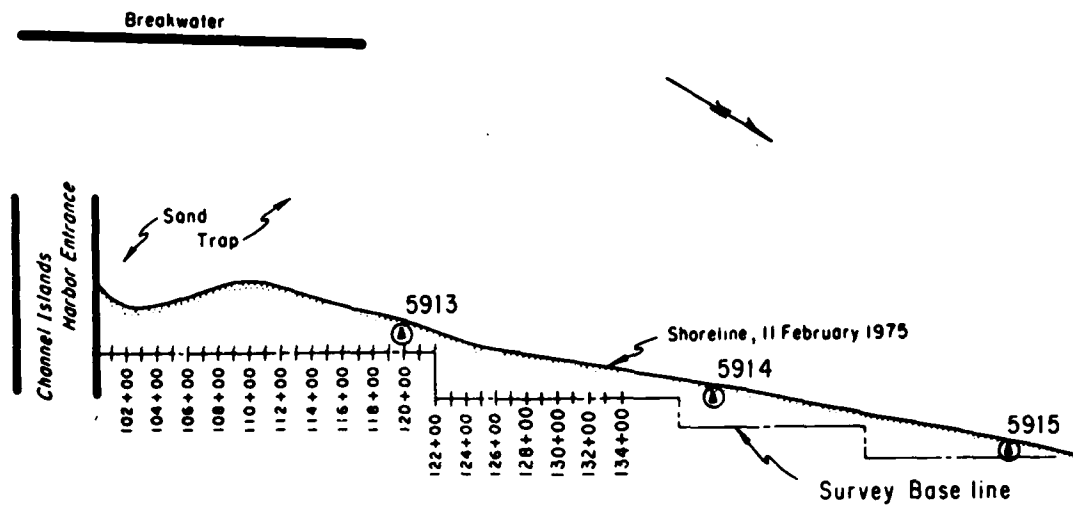


Figure 5. Longshore sand transport study, Channel Islands, 1976-77.

1. Bathymetric Survey Data Collection and Analysis.

U.S. Army Engineer District, Los Angeles assisted in the surveys. A base line was established approximately parallel to the shore, and profile lines normal to the base line were spaced at about 30.5 meters for a distance of about 823 meters (Fig. 6). Elevations at each station were measured from the base line out to the detached breakwater. Surveys were scheduled at 4- to 6-week intervals, but the scheduling was frequently modified due to survey crew availability, equipment failures, and unfavorable surf conditions.

Table 2 provides a summary of survey data, showing survey dates, ranges surveyed, type of fathometer calibration, survey method, and qualitative estimate of overall data quality. Under survey method, "standard" indicates an analog fathometer record was made, and the Los Angeles District's standard survey techniques were used to position the survey vessel. A man onshore directed the vessel operator along the profile line. At 10-second intervals, the analog recording was marked and the vessel position was recorded by plane table and alidade.



④ Indicates LEO Surf Observation Station

Figure 6. Longshore transport study area.

Table 2. Summary of survey data.

Date	Ranges surveyed	Fathometer calibration	Method used	Data quality
14 Apr. 1974	101+00 to 122+00	Leadline	Standard	5
7 May 1974	101+00 to 127+00	Leadline	Standard	6
18 June 1974	101+00 to 127+00	Leadline	Standard	0
30 July 1974	101+00 to 127+00	Leadline	Standard	7
20 Aug. 1974	101+00 to 127+00	Leadline	Standard	7
24 Sept. 1974	101+00 to 127+00	Leadline	Standard	7
6 Nov. 1974	101+00 to 127+00	Leadline	Standard	4
7 Jan. 1975	101+00 to 127+00	Leadline	Standard	5
11 Feb. 1975	101+00 to 122+00	Leadline	Standard	6
4 Mar. 1975	101+00 to 127+00	Leadline	Standard	7
27 Mar. 1975	101+00 to 127+00	Bar check	Hybrid	0
14 Apr. 1975	101+00 to 127+00	Bar check	Hybrid	7
6 May 1975	101+00 to 127+00	Bar check	Hybrid	8
1 Aug. 1975	101+00 to 127+00	Bar check	Standard	8
13 Aug. 1975	101+00 to 127+00	Bar check	Hybrid	8
16 Sept. 1975	101+00 to 127+00	Bar check	Hybrid	8
28 Jan. 1976	101+00 to 134+00	Bar check	Automated	8
20 Apr. 1976	101+00 to 134+00	Bar check	Automated	8
20 May 1976	101+00 to 134+00	Bar check	Automated	8
28 June 1976	101+00 to 134+00	Bar check	Automated	8
12 Aug. 1976	101+00 to 134+00	Bar check	Automated	8
8 Sept. 1976	101+00 to 134+00	Bar check	Automated	8
6 Oct. 1976	101+00 to 134+00	Bar check	Automated	8
1 Dec. 1976	101+00 to 134+00	Bar check	Automated	8
3 Feb. 1977	101+00 to 134+00	Bar check	Automated	8
22 Mar. 1977	101+00 to 134+00	Bar check	Automated	8
27 Mar. 1977	101+00 to 134+00	Bar check	Automated	8
6 June 1977	101+00 to 134+00	Bar check	Automated	8
21 July 1977	101+00 to 134+00	Bar check	Automated	8
30 Aug. 1977	101+00 to 134+00	Bar check	Automated	8

The "hybrid" method indicates an analog fathometer record was made and the survey vessel positioned by use of electronic ranging equipment. With this method, a man onshore directed the vessel operator along profile lines, but the vessel position was monitored by telemetering data to a field office where a real time plot of position was produced by a minicomputer. Monitoring the survey in progress determined and eliminated both errors in positioning. An electronic timer at 2-second intervals simultaneously marked the analog record and recorded the vessel's position on magnetic tape.

The "automated" method indicates that the soundings from the fathometer were digitized electronically and transmitted with position information to the field office minicomputer. All survey data soundings as well as position were monitored in real time.

A LARC 5 amphibious vehicle was used in all three methods for the bathymetric part of the survey. The LARC allows the continued measurement of the survey line through the surf zone, using rod and level methods when the vehicle's wheels contact the bottom. Profile lines over the dry beach areas were measured by standard level and rod transects.

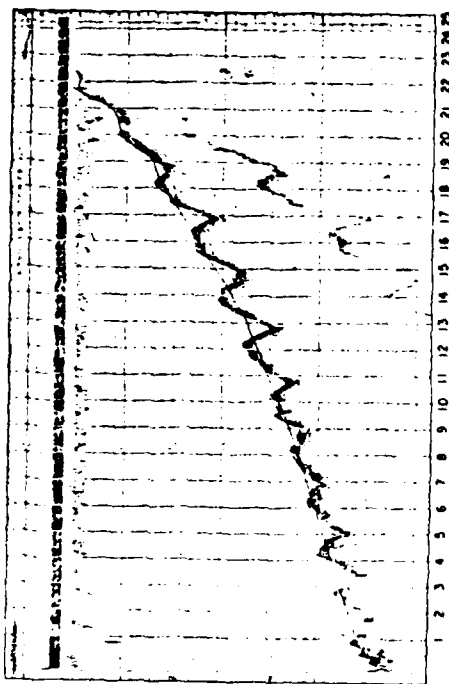
Late in phase I of the study, it was found the standard method was not providing the reliable, accurate data desired. As shown in the plots in Figure 7, the data are on a line sheltered by the breakwater and at a point beyond normal sand deposition. Divers measured the bathymetry using underwater reference stakes to verify no deposition at this point. These plots indicate that unacceptable errors were introduced on several surveys. These errors were a result of poor positioning data, poor fathometer calibrations, and errors in data reduction.

The standard surveying method assumes that the LARC is on line for all fixes and that the vessel's position and the fathometer record have been marked both precisely and simultaneously. However, this is not always true and errors that occur can never be recovered. Even with no errors produced in field collection, reduction of working scale plane-table data sheets was limited to an accuracy of about 3 meters which was seldom attained.

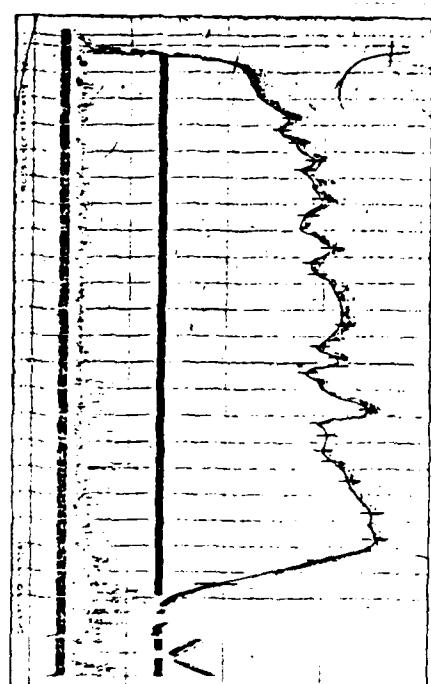
In the hybrid method, an electronic timer simultaneously marked the fathometer at 2-second intervals and controlled the recording of the LARC's position, eliminating human errors in determining position. Position accuracy, which was limited by the electronic ranging equipment, was about 2 meters and consistently attained.

During the surveys, errors were also produced in fathometer calibrations and data reduction procedures. Under the standard method, leadline soundings were used for the first year (April 1974 to March 1975) for fathometer calibration. In taking leadline soundings, accuracy is determined by numerous factors, including skill and care of the operator, motion of the vessel, and roughness of the water's surface. Later surveys used a bar lowered at 5-foot intervals under the fathometer for calibration. This type of calibration (bar check) eliminates human factors and is complete in that it shows any occurrence of nonlinearity in the fathometer.

Uncertainty in interpreting the fathometer records is another source of error which was discovered. Figure 8 shows fathometer records of two profiles,



RANGE 124+00 - FATHOMETER RECORD WITH WAVES



RANGE 104+00 - FATHOMETER RECORD WITHOUT WAVES
Figure 8. Fathometer record of regular bottom with waves and irregular bottom without waves.

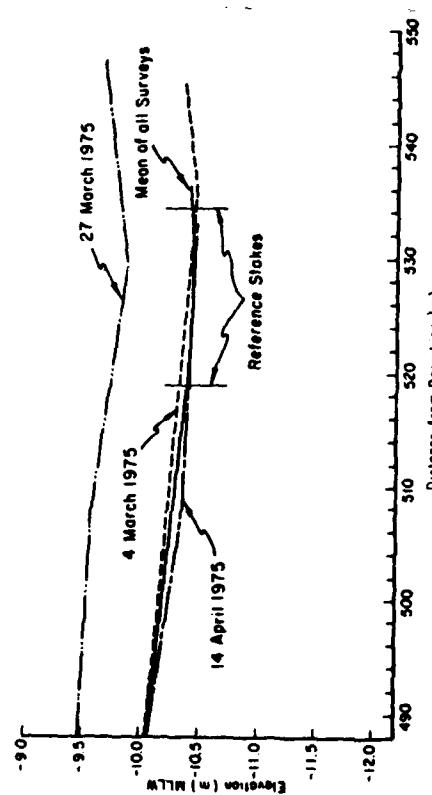
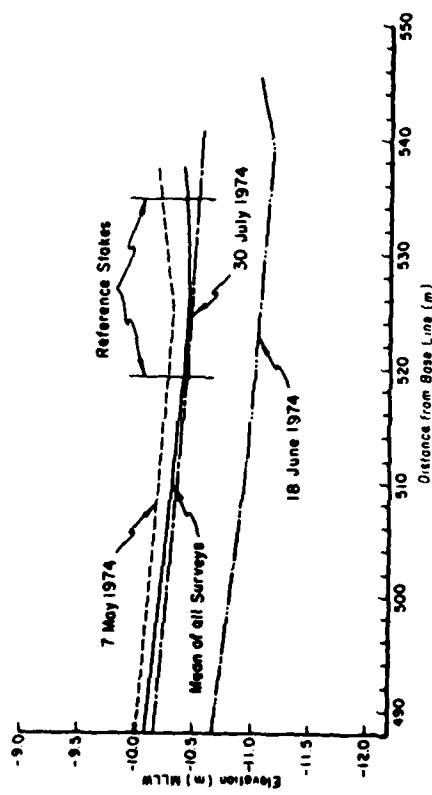


Figure 7. Illustrations of survey errors at reference station.

both with similar features which appear to be waves; however, on one record these features indicate the irregular bottom left after dredging. For this reason, all data reduction under the hybrid method was performed by the field investigators who observed conditions at the time of data collection. Also, this possible misinterpretation was the reason no smoothing was done under the automated method.

The data quality rating in Table 2 is a subjective rating, from 0 (poor) to 10 (good), determined by the field investigators after examining the data on hand, field notes, and all profile plots. Using this approach, it was determined that data collected 18 June 1974 and 27 March 1975 (see Fig. 7) were unreliable (Table 2).

In the survey analysis, deposition from upcoast (northerly) transport during times of reversals in wave direction and possible deposition due to reversals in the area of the trap seaward and upcoast of the jetties were examined. Figure 9 is a plot of the first profile upcoast of the jetties. Survey dates of 17 April 1974 and 16 September 1975 are plotted, showing the total change at this profile over that period. The plot shows little deposition at the end of the jetty. All profile data were examined in detail to define the area of deposition attributable to influx of material from north (upcoast) to the trap. No significant deposition was measured at distances more than 485 meters from the base line. Using this distance (485 meters) from the base line as an outward boundary to calculate volumes, errors due to influx of material from reversals were minimal.

Volume changes were calculated, using the area between the base line and 485 meters offshore and the north jetty and 670 meters upcoast. Over this area a volume accuracy of within $\pm 5,000$ cubic meters was expected when survey errors had been minimized.

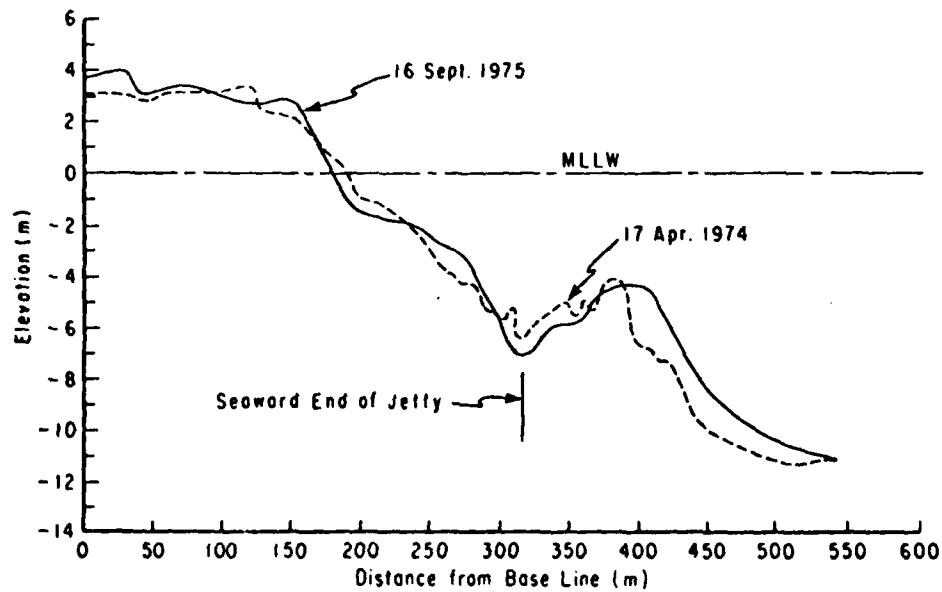


Figure 9. Range 101+00 at beginning and end of study.

Figure 10 shows bottom changes at station 109+00 (midprofile of the trap area) between April 1974 (immediately after dredging in phase I of the study) and July 1974 (4 months later) surveys. Predredging conditions in September 1973 are also shown.

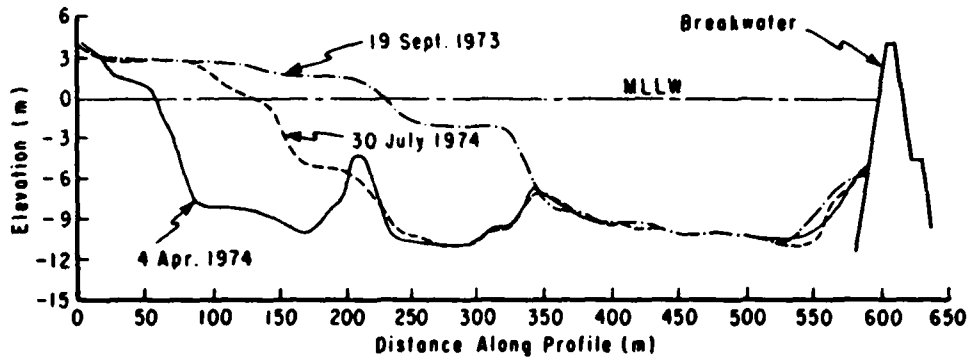


Figure 10. Profile changes at range 109+00.

Figure 11 shows bathymetric changes within the sand-trap area from 17 April to 30 July 1974; only major changes in bathymetry are reflected due to contouring at 1-meter intervals. The map indicates a zone of deposition from stations 102+00 and 122+00 along the shore and 30 to 300 meters seaward of the working base line. The figure is representative of the type of filling the sand trap experienced during the entire project study. Most of the sand-trap deposition occurred well within 300 meters of the shoreline.

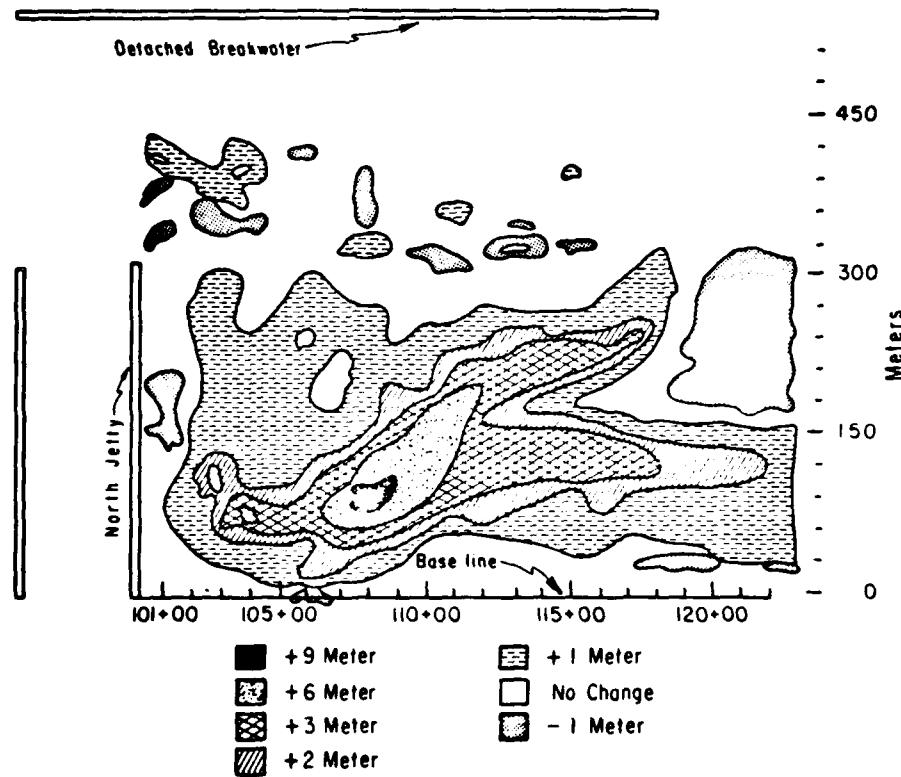


Figure 11. Elevation changes between 17 April and 30 July 1974 surveys.

2. LEO Data Collection and Analysis.

Figure 6 shows three sites where twice daily surf data were collected using procedures developed under the CERC LEO program (Bruno and Hiipakka, 1973; Berg, 1968). These data include observations of surf conditions, local winds, and littoral currents. The primary concern of this study was the estimates of breaker height, breaker direction, and longshore current. To aid in estimating the breaker direction, LEO observers were provided with a protractor on the data form. Longshore currents were measured using small packets of dye which disperse upon injection in the surf zone. The observers measure the distance the dye travels parallel to the shoreline. Current speed is estimated from the movement of the dye patch centroid over a 1-minute period, and current direction is noted. Surf zone current velocities are not uniform; therefore, the width of the surf zone is estimated as well as the distance from the shoreline to the point of dye injection.

LEO data were used to compute the longshore energy flux factor, using two methods of computation, in order to relate the wave energy to the longshore sediment transport. The first method involved the typical approach to computing the longshore energy flux, using wave heights and wave angles at breaking. This method utilizes the SPM equation (4-29):

$$P_{LS} = \frac{\rho g H_b^2}{16} C \sin 2\alpha_b \quad (5)$$

where

P_{LS} = longshore energy flux factor

ρ = fluid density

H_b = breaking wave height

α_b = breaking wave angle

C = group wave velocity at breaking.

Using linear wave theory, shallow-water assumption and a linear relationship between breaking wave heights and depth equal to

$$\kappa = \frac{H_b}{d_b} \quad (6)$$

where d_b = breaking wave depth, equation (5) becomes

$$P_{LS} = \frac{\rho g}{16} H_b^{5/2} \left(\frac{g}{\kappa} \right)^{1/2} \sin 2\alpha_b \quad (7)$$

The longshore energy flux computed from equation (7) is dependent on only two surf zone parameters--breaking wave height and breaking wave angle. The assumed value of κ for computation, $\kappa = 0.78$, is reasonable for various monochromatic wave theories (e.g., see Longuet-Higgins, 1970). The breaking wave height measured by LEO observers is assumed to be the significant wave height

(average of the highest one-third of the waves). In this study it was desired to compute the "true" wave energy flux; therefore, wave height was modified to reflect the root-mean-square (rms) wave height in accordance with the statistical wave train theory of Longuet-Higgins (1967) assuming a narrow-banded wave energy spectrum. For this particular situation, which results in a Rayleigh probability distribution for wave height, the relationship between significant wave height and rms wave height is as follows:

$$H_s = (2)^{1/2} H_{rms} \quad (8)$$

where H_s is the significant wave height, and H_{rms} the root-mean-square wave height.

The second method computes longshore energy flux, using breaker wave height and longshore current as determined from LEO measurements, along with estimated values of surf zone width, W , and distance from shoreline to injection point of dye, X . The equation for determining longshore energy flux using this second method is

$$P_{ls} = \frac{\rho g H_b W V C_f}{\frac{5\pi}{2} \kappa \left(\frac{V}{V_o}\right)_{LH}} \quad (9)$$

where V is the longshore velocity as measured in LEO program, C_f the friction coefficient dependent on bottom water particle excursion bottom roughness, and $(V/V_o)_{LH}$ the theoretical dimensionless longshore velocity for Longuet-Higgins' assumed mixing parameter, $P = 0.4$; $(V/V_o)_{LH}$ is dependent on the parameter X/W (see Longuet-Higgins, 1970).

The derivation of equation (9) is given in Appendix A. The rms wave height is used in equation (9) to calculate the longshore energy flux. Longshore velocity is typically measured over a timespan on the order of the "modulated" wave train period.

In this part of the study, additional emphasis was placed on determining a reasonable bottom friction coefficient, C_f , for use in equation (9). The friction coefficient was determined by minimizing the variance between computed longshore currents (from LEO observation) and theoretical longshore currents (from Longuet-Higgins' (1970) formula with an assumed mixing coefficient $P = 0.4$). LEO data from the two northernmost LEO stations (out of the zone of breakwater influence) were chosen for the calculation. More than 2 years of twice daily wave observations (4,464 observations) from the two stations was used to compute the friction coefficient, $C_f = 0.0056$, which was used in equation (9) to calculate the longshore energy flux.

In both methods, weighted averages of the longshore energy flux at breaking are calculated which correspond to periods between volumetric surveys. Values of P_{ls} are given for the three stations in Appendix B, Tables B-1 and B-2. In most survey periods, the value of P_{ls} computed from current data was higher than the value of P_{ls} calculated using wave angle information. In addition to longshore energy flux, correlation coefficients R are also calculated for the correspondence between calculated longshore currents (from Longuet-Higgins' (1970) theoretical approach) and measured longshore currents. Correlation coefficients ranged from -0.18 to 0.76 and are independent of assumed friction factor.

In assessing the data for use in predicting sand transport, it is pertinent to assess the quality of the LEO data from the standpoint of consistency, both spatially and temporally. Values of P_{ls} computed from LEO stations 5714 and 5715 (Fig. 6, two northernmost stations) show surprisingly good agreement when comparing similarly computed values within the same time frame (either current or wave angle). This correspondence also holds for station 5713 which is only 90 meters north of the north end of the Channel Islands offshore breakwater. It is believed that station 5713 observations were strongly affected by diffraction effects caused by the breakwater. Station 5713 data were not used in any of the correlations between the longshore energy flux and sand transport discussed later in this report.

To indicate temporal consistency of the data source, average P_{ls} values (for stations 5714 and 5715) were plotted versus time (in months) for the two phases of the study (Fig. 12). Comparing the two phases in the figure shows that the low wave energy periods occur consistently during the summer and early fall months.

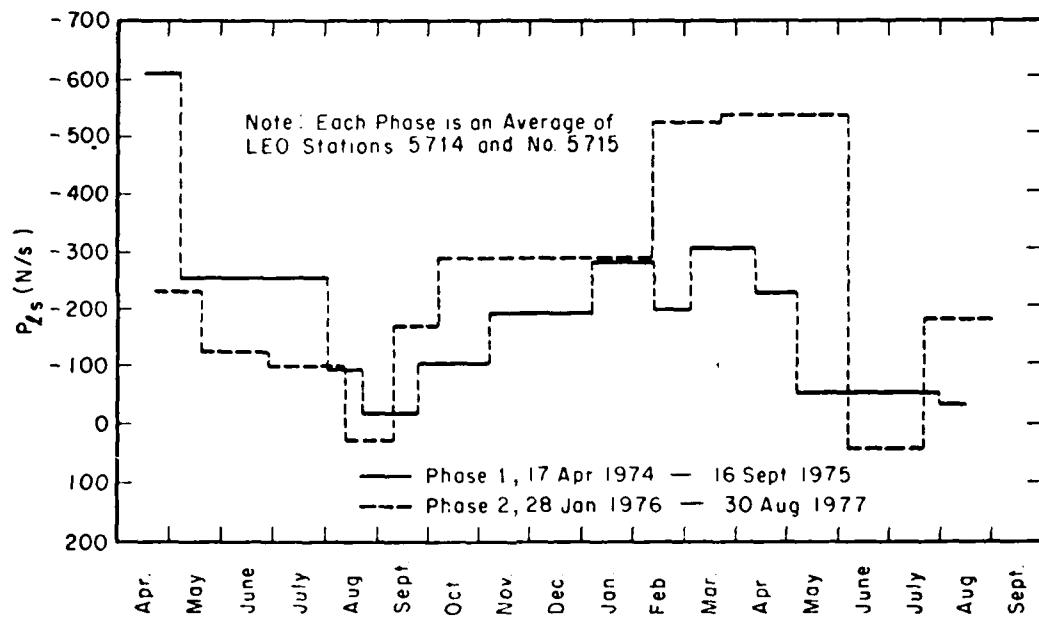


Figure 12. Net longshore energy flux versus time for LEO stations 5714 and 5715.

Correlation between the weighted average longshore energy flux and the longshore sand transport is discussed in a later section of this report. Problems arose when reversals in wave direction (and consequently the longshore energy flux) occurred, due to the limited extent of the survey area in which accretion was always dominant. As a result, there were periods in which both the weighted average longshore energy flux and the volume change were positive (northward-directed energy flux and accretion). This apparent discrepancy was due to the limited extent of the survey area north of the offshore breakwater which was still trapping sand even though northward of the survey area, the sand transport was in a northerly direction. This overtrapping effect is due to wave diffraction patterns caused by the breakwater driving sand into the sheltered area behind the breakwater. In these particular cases, no correlation

could be made. Thus, the effects of a strong reversal in wave climate must also be considered in the other data since an evenly balanced wave climate with a preponderance of southward-directed energy flux (which would give a low negative "net" P_{Ls} value) might be correlated with an excessively large volumetric accretion. To assess the possibility of this phenomena, the ratio of the cumulative total northward energy flux to the cumulative total southward energy flux was calculated for the average P_{Ls} value of stations 5714 and 5715. This ratio is presented in Appendix B, Table B-3, and is discussed later in this report.

At the end of phase I of the study, LEO wave observations were compared to the wave gage significant wave heights to determine any inconsistencies in the LEO recorded waves. Figure 13 provides the comparison, for a 6-month period during phase I of the study, which shows that the observer consistently recorded lower wave heights than the gage recorded in the case of the higher waves. Although the plotted gage wave heights have not been modified to reflect a breaking wave height, an analysis of the transformation to breaking conditions in a few selected cases did not alter the results significantly. This observer bias in underestimating the higher waves was found to result from the observer practice of recording the last breaking wave closest to the shoreline in the case of multiple-breaking waves. Thus, when the higher waves broke offshore, re-formed, and then broke again, the observer was only recording the last and closest (to the observer) breaking wave height.

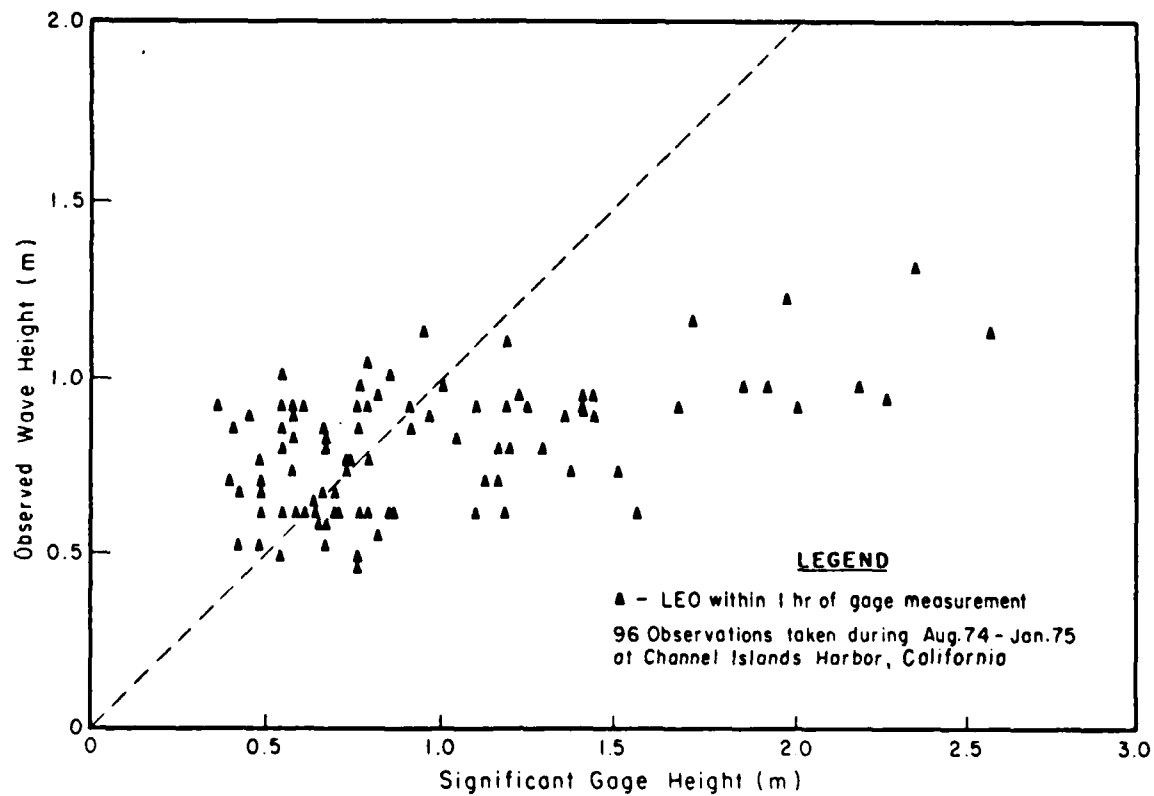


Figure 13. Comparison of observed wave heights (LEO) to recorded wave gage heights in phase I of study.

In phase II of the study the observer had been requested in estimating wave heights to record the outer breaker. As a result, a comparison of LEO wave height measurements and wave gage measurements in phase II gave a much better correlation (see Fig. 14).

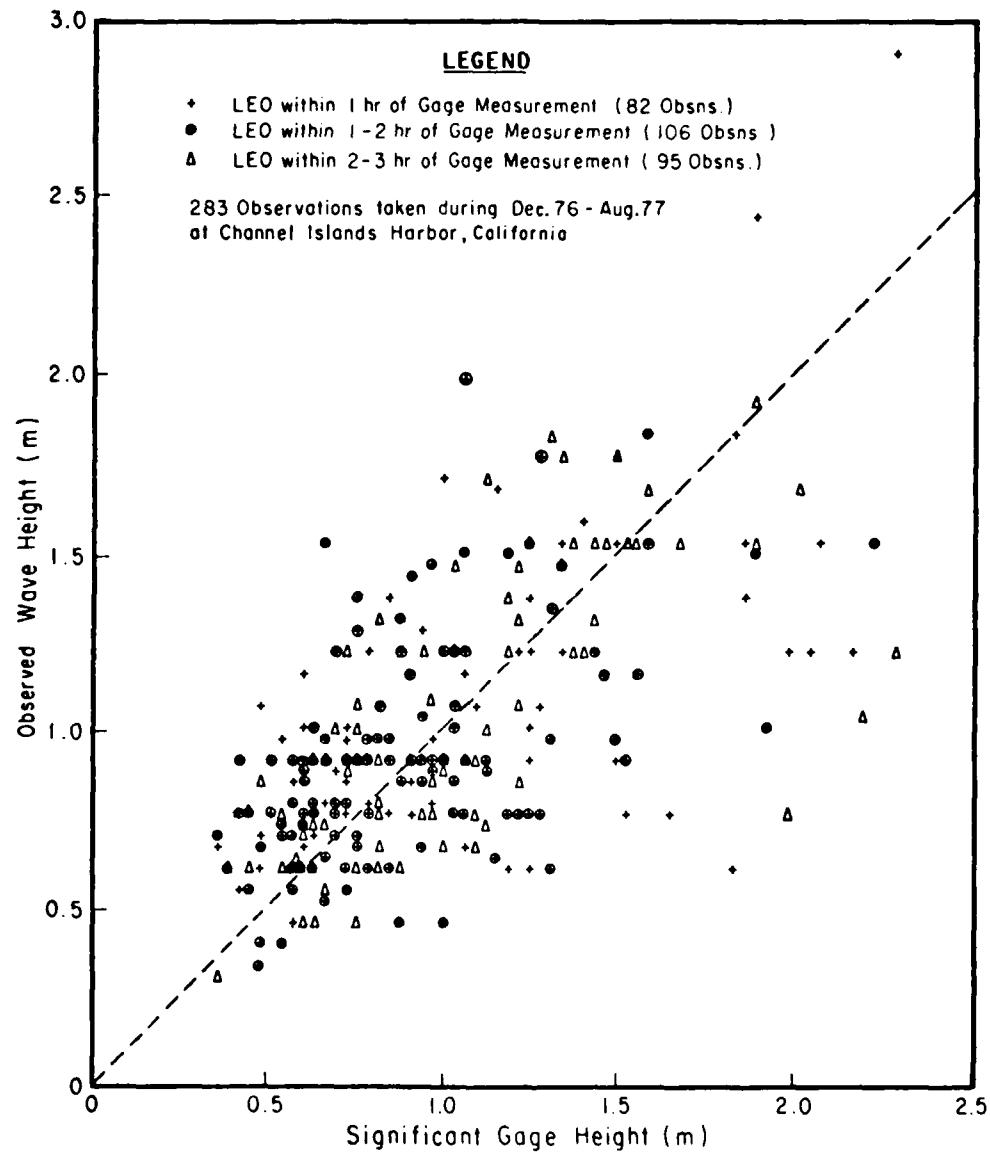


Figure 14. Comparison of observed wave heights (LEO) to recorded wave gage heights in phase II of study.

The strong dependence of the longshore energy flux on wave height ($P_{ls} \sim H^{5/2}$, eq. 7; $P_{ls} \sim H$, eq. 9) necessitated disregarding the LEO data in phase I and using only the wave gage directional spectra for sand transport correlations.

In comparing the calculated values of longshore energy flux from the two methods, the wave angle method (eq. 7), and the longshore current method (eq. 9), it was found that the longshore current method led to higher values of longshore energy flux during most data periods. The reason for this is unknown.

3. Wave Gage Data Collection and Analysis.

During the period 30 July 1974 to 6 May 1975, two total pressure sensors were located near the bottom in an approximate 6-meter water depth, separated by approximately 23 meters; the geometric characteristics of the gage installations are presented in Figure 15. Pressure records, which were recorded in digital form approximately every 2 hours, contained 4,096 data points at 0.25 seconds each, resulting in a record length of 17.07 minutes. In order to calculate P_{ls} at breaking, the following steps were carried out: (a) Calculation of the frequency-by-frequency wave direction and energy at the location of the wave gages; (b) transformation of the wave spectrum to the breaker line, including shoaling and refraction effects; and (c) computation of P_{ls} at the surfline. Each of these is described below.

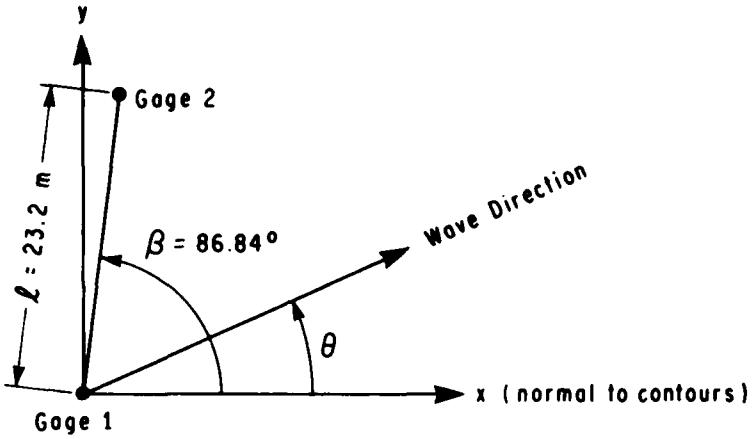


Figure 15. Characteristics of a two-gage array at Channel Islands Harbor, California.

a. Calculation of Wave Characteristics at Wave Gages. The pressure time series were analyzed using a standard fast Fourier transform (FFT) program to determine the coefficients. For example, the time series from gage 1 is represented by

$$P_1(t_j) = \sum_{n=0}^{N-1} [a_1(n) - ib_1(n)] e^{\frac{i2\pi nj}{N}} \quad (10)$$

in which $i = \sqrt{-1}$, and N is the total number of data points ($N = 4,096$) for each gage.

The FFT coefficients are defined in terms of the pressure time series as

$$a_1(n) - ib_1(n) = \frac{1}{N} \sum_{j=1}^N P_1(t_j) e^{-\frac{i2\pi nj}{N}} \quad (11)$$

and the $a_1(0)$ term represents the mean of the record. In calculating the FFT coefficients, there are a large number of "tapers" (or windows) that may be used to reduce the adverse effects of spectral leakage which arises due to representing an aperiodic time series by a periodic series (Harris, 1976). These tapers all have the form

$$P'(t_j) = w(j)p(t_j) \quad (12)$$

in which $p(t_j)$ is the measured pressure, and $w(j)$ is a weighting factor. A characteristic of these tapers is that they are unity at the midpoint of the time series and decrease to a lesser value near the two ends. In the present analysis, it was determined through a number of test calculations that although the effect of tapering at an individual frequency could be substantial, the overall effect on P_{LS} was quite small, generally less than 4 percent. Thus, no taper was used in the analysis.

The depth of water, Δd , overlying the pressure sensors is obtained from $a_1(0)$ and $a_2(0)$ as

$$\Delta d = \frac{0.5}{\gamma} [a_1(0) + a_2(0)] \quad (13)$$

in which γ is the specific weight of seawater. The total water depth, d , is the sum of Δd and the distance, S_G , of the pressure sensors above the bottom (0.3 meter).

Each FFT pressure coefficient is transformed to a water surface displacement coefficient by the following linear wave theory relationship:

$$[a_n(n), b_n(n)] = \frac{1}{\gamma K_p(n)} [a_p(n), b_p(n)] \quad (14)$$

in which $K_p(n)$ is

$$K_p(n) = \frac{\cosh k_n(S_G)}{\cosh k_n d} \quad (15)$$

In equation (15), k_n is the wave number associated with the angular frequency, σ_n , as obtained from the linear wave theory dispersion relationship

$$\sigma_n^2 = gk_n \tanh k_n d \quad (16)$$

One disadvantage of measuring waves with near-bottom pressure sensors is evident by examining equations (14) and (15). For higher frequencies (shorter wave periods) K_p is very small, resulting in very small pressure fluctuations near the sea floor for the higher frequency waves. Thus, to avoid contaminating the calculated water surface displacement, η , it is usually necessary to apply a high-frequency cutoff above which the pressure contributions are discarded. The proper selection of this high-frequency cutoff depends on the signal-to-noise characteristics of the pressure sensor and signal conditioning system. For the present analysis, the high-frequency cutoff was established at a wave period of 3.1 seconds. For a nominal 6-meter water depth and a 0.3-meter height of the pressure sensor above the bottom, the pressure signal is attenuated to approximately 16 percent of its surface value. In the survey area, where reasonably long Pacific swells occur, neglecting wave energy for periods shorter than approximately 3 seconds appears justified.

Denoting hereafter the FFT coefficients for the water surface displacement as $a(n)$ and $b(n)$, it is noted that the coefficients have the following properties:

$$\overline{\eta^2} = \sum_{n=1}^{N-1} [a^2(n) + b^2(n)] \quad (17)$$

$$\left. \begin{aligned} \frac{a_N}{2} + k &= \frac{a_N}{2} - k \\ \frac{b_N}{2} + k &= -\frac{b_N}{2} - k \end{aligned} \right\} \quad (18)$$

and thus

$$\overline{\eta^2} = 2 \sum_{n=1}^{N/2} [a^2(n) + b^2(n)] \quad (19)$$

Therefore, the total (kinetic plus potential) energy, $E(n)$, associated with a particular frequency component, n , is

$$E(n) = 2\gamma[a^2(n) + b^2(n)] \quad (20)$$

For wave direction, consider the definition sketch in Figure 16 and the following representation for $\eta(x, y, t_j)$:

$$\begin{aligned} \eta(x, y, t_j) &= \sum_{n=1}^N F(n) e^{\frac{i2\pi nj}{N}} - [k_x(n) \cos \alpha(n) \cos \alpha(n) + k_y(n) \sin \alpha(n) - \epsilon(n)] \\ &= \sum_{n=1}^N [a(n) - ib(n)] e^{\frac{i2\pi nj}{N}} \end{aligned} \quad (21)$$

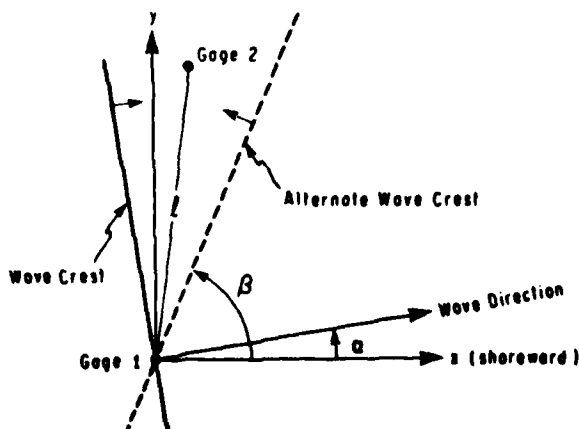


Figure 16. The two-gage array notation and directional ambiguity.

Denoting the water surface displacements at the two gage locations as $\eta(x_1, y_1, t)$ and $\eta(x_2, y_2, t)$ and calculating the cross spectrum, $S_{12}(n)$,

$$S_{12}(n) = \overline{[a_1(n) - ib_1(n)]} [a_2(n) - ib_2(n)] \quad (22)$$

where the overbar denotes the complex conjugate,

$$\begin{aligned} S_{12}(n) &= [a_1(n)a_2(n) + b_1(n)b_2(n)] - i[a_2(n)b_1(n) - a_1(n)b_2(n)] \\ &= c_{12}(n) - iq_{12}(n) \end{aligned} \quad (23)$$

and $c_{12}(n)$ and $q_{12}(n)$ are the "cospectrum" and "quadspectrum," respectively of η_1 and η_2 . $S_{12}(n)$ can also be expressed as

$$\begin{aligned} &-i[k_n(x_2 - x_1) \cos \alpha(n) + k_n(y_2 - y_1) \sin \alpha(n)] \\ S_{12}(n) &= F^2(n)e \end{aligned} \quad (24)$$

and noting from Figure 16 that the separation distance and orientation of a line joining the two gages are denoted by ℓ and β , respectively, $S_{12}(n)$ can be written as

$$\begin{aligned} &-ik_n\ell \cos [\alpha(n) - \beta] \\ S_{12}(n) &= F^2(n)e \\ &= F^2(n) \cos \left\{ k_n\ell \cos [\alpha(n) - \beta] \right\} - iF^2(n) \sin \left\{ k_n\ell \cos [\alpha(n) - \beta] \right\} \end{aligned} \quad (25)$$

Comparing equations (23) and (25), it is apparent that the wave direction, $\alpha(n)$, relative to the x-axis can be expressed as

$$\alpha(n) = \beta \pm \cos^{-1} \left\{ \frac{1}{k_n\ell} \tan^{-1} \left[\frac{q_{12}(n)}{c_{12}(n)} \right] \right\} \quad (26)$$

where the \pm is the result of a directional ambiguity associated with a two-gage array (Fig. 16) and is avoided by choosing the minus sign which selects the wave arriving from the seaward half-plane adjacent to a line joining the two gages.

There are two conditions for which it was not possible to calculate the wave direction, $\alpha(n)$: (1) poorly conditioned wave data, presumably due to spectral leakage, and (2) spatial aliasing due to the fairly large separation distance (≈ 23 meters) between the two gages. If the first condition exists, the absolute value of the quantity within the brackets {} in equation (26) may exceed unity, clearly a physically impossible condition since the extreme values of the cosine function are ± 1 . This tended to occur for very long waves for which both the energy and the value of k_n were small. The percentage of energy within an individual record when this condition occurred was relatively small, averaging 2 to 3 percent with a maximum of approximately 10 percent. The second condition requires that the wavelength be equal to or greater than twice the projection of the wave gage separation distance in the direction of wave propagation. Referring to Figure 16

$$L > 2\ell [\cos(\alpha - \beta)]_{\max} \quad (27)$$

which indicates that for the least adverse effects of spatial aliasing, the gages should be aligned parallel to the dominant orientation of the wave crests. In the present case $\beta = 86.8^\circ$ and, in general, the waves approached within approximately 40° of the shoreline. In the analysis, a variable aliasing frequency limit depending on the wave directions for the lower frequencies was developed for each record. Three frequency limits were considered, corresponding to $|\alpha - \beta|$ values of 45° , 60° , and 75° , with the 75° value associated with the highest frequency limit. Selection of the frequency limit required that 90 percent of the wave energy in a frequency range $\sigma_A/2$ to σ_A lay within the associated wave direction range, where σ_A is the frequency corresponding to the particular aliasing wave direction (eq. 27). For the water depth at the site, the three directional limits of 45° , 60° , and 75° are associated with approximate wave periods of 5.3, 4.2, and 3.1 seconds, respectively. The percentage of energy associated with periods shorter than 5.3 seconds was substantial in the data, amounting to 25 to 30 percent. In later calculations of P_{ls} , an attempt was made to account for the energy above the aliasing frequency by augmenting the calculated values, using

$$P_{ls_{cm}} = P_{ls_c} \frac{E_{TOT}}{E} \quad (28)$$

in which the subscripts c and cm indicate calculated and calculated modified, respectively. E_{TOT} and E represent the total wave energy values and the energy below the spatial aliasing frequency. This modification is equivalent to associating the effective direction as determined from the frequencies not affected by the aliasing consideration or poorly conditioned data to all the wave energy.

b. Determination of Breaking Depth. At this stage, the wave energy and wave direction in the vicinity of the gages are determined. These values are then transformed to the breaker line, accounting for shoaling and refraction.

To determine a breaking depth, a method was used in which the total onshore flux of wave energy was equated at the gages and at the breaker line with the requirement that the rms breaking wave height, H_{rms} , be related to the water depth by

$$H_{rms} = \kappa d_b \quad (29)$$

in which κ was taken as the usual spilling breaker value of 0.78. The total onshore energy flux, F_R , at the reference (gage) location is

$$F_R = 2\gamma \sum_{n=1}^{N/2} [a^2(n) + b^2(n)] C_g(n) \cos \alpha_n \quad (30)$$

in which the subscript R denotes the reference location. Considering shallow-water conditions for breaking $C_g(n) = C = \sqrt{gd_b}$ and $\cos \alpha_b \approx 1.0$, the onshore energy flux at breaking is

$$F_b = \frac{\gamma H_b^2}{8} \sqrt{gd_b} = \frac{\gamma k^2}{8} \sqrt{gd_b}^{2.5} \quad (31)$$

Equating F_R and F_b

$$d_b = \left\{ \frac{16 \sum_{n=1}^{N/2} [a^2(n) + b^2(n)] C_g(n) \cos \alpha_n}{k^2 \sqrt{g}} \right\}^{0.4} \quad (32)$$

Note that neglecting wave refraction in the breaking depth determination does not result in very large errors; e.g., for a wave direction at the gages of 30° , the error in breaking depth would be less than 6 percent. For a more realistic overall wave direction of 20° , the associated error in breaking depth is less than 3 percent.

c. Transformation of Wave Components to Shore. With the breaking depth known, each wave component is transformed to shore, accounting for both wave refraction and shoaling as based on linear wave theory. Wave refraction was computed in accordance with Snell's law and the assumption that straight and parallel contours existed between the gage and breaking locations,

$$\alpha_b(n) = \sin^{-1} \left[\frac{C_b(n)}{C_R(n)} \sin \alpha_R(n) \right] \quad (33)$$

Shoaling was based on linear theory, resulting in the value of the sums of the squared FFT coefficients at the breaker line of

$$[a^2(n) + b^2(n)]_b = \frac{\cos \alpha_R(n)}{\cos \alpha_b(n)} \frac{[C_g(n)]_R}{[C_g(n)]_b} [a^2(n) + b^2(n)]_R \quad (34)$$

in which the first and second ratios on the right side of the equation represent the effects of refraction and shoaling, respectively.

d. Computation of P_{ls} at the Surfline. With the wave energy and direction known at the breaker line, the value of the wave energy flux factor, P_{ls} , is readily determined.

$$P_{ls} = G \left\{ 2 \gamma \sum_{n=1}^{N/2} [a^2(n) + b^2(n)]_b C_{gb}(n) [\cos \alpha(n) \sin \alpha(n)]_b \right\} \quad (35)$$

where the factor G is given by the ratio

$$G = \frac{E_{TOT}}{E} \quad (36)$$

as defined in and discussed in relation to equation (28).

e. Orientation of Wave Gages. In calculating directional wave properties relative to the shoreline, it is extremely important to establish the orientation of the wave gage array and a representative shoreline orientation. During the original study, the locations of the wave gages had been established by measuring angles with transits from two known shore stations on the project base line. These angles were then translated into gage locations through standard geometric procedures. Two sets of such measurements were taken on 24 and 26 June 1974. The resulting gage characteristics are presented in Table 3.

Table 3. Geometric characteristics of the two-gage array.

Date	Gage separation distance (m)	Gage orientation with respect to base line
24 June 1974	23.55	10.81°
26 June 1974	22.71	14.44°
7 June 1980		
Trial 1	23.8	15.81°
Trial 2	23.2	12.74°
Trial 3	22.6	12.36°
Values adopted in this study	23.2	13.23°

Although the gage separation distances obtained from the two surveys differed somewhat more than desired, the gage orientations that differed by 3.6° were of particular concern. Thus, on 7 June 1980, these variables were established using range-range microwave equipment. Measurements were obtained from three combinations of shore-based locations, which allowed a better determination of gage orientation; the results are also presented in Table 3. The average of all values were adopted for the present study.

f. Effective Shoreline Orientation. The determination of effective shoreline orientation was somewhat more difficult at this site than originally anticipated. One difficulty was that dredging and subsequent filling by longshore sediment transport in the impoundment area caused local anomalies in the bottom contours, such that they were not quite straight and parallel. In particular, following a dredging activity, the nearshore contours moved landward more than the seaward contours. This is believed to be an expression of the concentration of the longshore sediment transport in the nearshore zone.

The shoreline orientation was established by plotting and overlaying profiles located in the vicinity of the wave gages. The relative landward-seaward locations of the profiles were adjusted in the overlays to obtain best agreement by eye and the associated orientation determined. A range of orientations were obtained by matching the nearshore and offshore parts of the profiles. These ranges were qualitatively consistent with those determined from aerial photography, with the larger angles associated with the more seaward parts of the profiles (see Table 4).

Table 4. Shoreline orientation as determined from beach and offshore profiles.

Date of survey	Range of effective shoreline orientation relative to base line
8 May 1974	9.95° to 11.33°
18 June 1974	8.83° to 10.78°
Value adopted in this study	10.07°

4. Results of Longshore Sand Transport-Longshore Energy Flux Factor Correlation.

In the correlation of P_{ls} with I, only the values directed toward the trap were used. The rationale is that during all periods when waves were directed toward the trap, there was sediment available for transport; therefore, this variable provides the best basis for correlation.

The volumetric accumulations were interpreted as I values by equation (3), using $p = 0.35$, and by dividing the time (in seconds) between surveys.

In phase I of the study (April 1974 to September 1975), the available values of longshore energy flux factor were computed using wave gage data. Longshore energy flux factors were also computed using LEO data during the same period but, as discussed previously, for higher waves the LEO wave heights, in comparison with wave gage data, were typically underestimated so the LEO data were not used in phase I. The wave gage data were available nominally every 2 hours. The value of P_{ls} for a survey period was obtained by summing all P_{ls} values directed toward the trap and dividing by the total number of wave recordings.

In phase II (January 1976 to August 1977), only data from one wave gage were available for a limited time; therefore, it was not possible to analyze directional wave spectra to compute the longshore energy flux factor. As discussed earlier, the LEO wave height observations during phase II did correlate reasonably well with wave gage data. As a result, the longshore energy flux factor was computed using LEO data and the LEO current method presented in equation (9).

Table 5 provides a summary of the analyzed data in phases I and II. Figure 17 presents the same data along with the SPM volumetric sand transport relationship converted to the more common relationship of equation (1) between the longshore energy flux factor and the immersed weight sand transport rate (in metric units). In this relationship, the constant K is dimensionless and ranges from 0.42 to 1.51 in the phase I data and from 0.19 to 4.18 in the phase II data. The average value for the two sets of data is $\bar{K} = 0.98$ with a breakdown for the two sets as follows:

Phase	No. of data	\bar{K}	σ_K	$\sigma_K/\bar{K} \times 100$ (pct)
I	7	0.87	0.33	38
II	11	1.05	1.08	103

Table 5. Summary of analyzed data.^{1,2}

Survey period	I (N/s)	P_{ls} (N/s)	$P_{ls\ net}$ (N/s)	Wave data source
Phase I				
30 July to 20 Aug. 1974	182.1	-120.3	-70.4	Wave gages(2)
20 Aug. to 24 Sept. 1974	144.6	-153.5	-107.3	Wave gages(2)
24 Sept. to 6 Nov. 1974	171.2	-295.8	-137.6	Wave gages(2)
6 Nov. 1974 to 7 Jan. 1975	439.3	-426.8	-345.9	Wave gages(2)
7 Jan. to 11 Feb. 1975	401.4	-446.6	-466.6	Wave gages(2)
11 Feb. to 4 Mar. 1975	245.8	-330.9	-186.4	Wave gages(2)
4 Mar. to 14 Apr. 1975	326.2	-782.8	-753.8	Wave gages(2)
Phase II				
20 Apr. to 20 May 1976	113.8	-204.4	-197.6	LEO
20 May to 28 June 1976	198.8	-114.4	-109.3	LEO
28 June to 12 Aug. 1976	136.5	-108.2	-81.9	LEO
12 Aug. to 8 Sept. 1976	107.6	-25.7	+24.1	LEO
8 Sept. to 6 Oct. 1976	176.1	-187.4	-143.1	LEO
6 Oct. to 1 Dec. 1976	48.9	-250.4	-242.4	LEO
1 Dec. 1976 to 3 Feb. 1977	141.9	-279.2	-245.7	LEO
3 Feb. to 22 Mar. 1977	352.2	-469.2	-443.1	LEO
22 Mar. to 6 June 1977	191.2	-460.0	-446.0	LEO
6 June to 21 July 1977	66.7	-77.9	+34.8	LEO
21 July to 30 Aug. 1977	35.2	-184.3	-153.3	LEO

¹Negative values of longshore energy flux factor, P_{ls} , represents flux toward the sand trap.

² P_{ls} values using wave data were calculated in accordance with equation (35); P_{ls} values using LEO observations were calculated using equation (9).

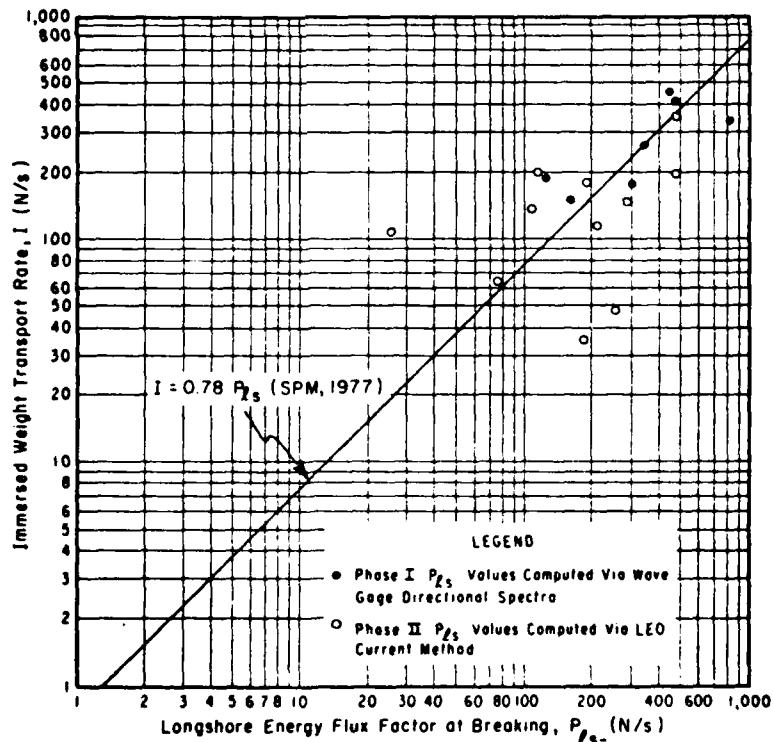


Figure 17. Sediment transport energy flux relationship for Channel Islands study.

Figure 18 presents the present data set along with the data set used in the SPM relationship.

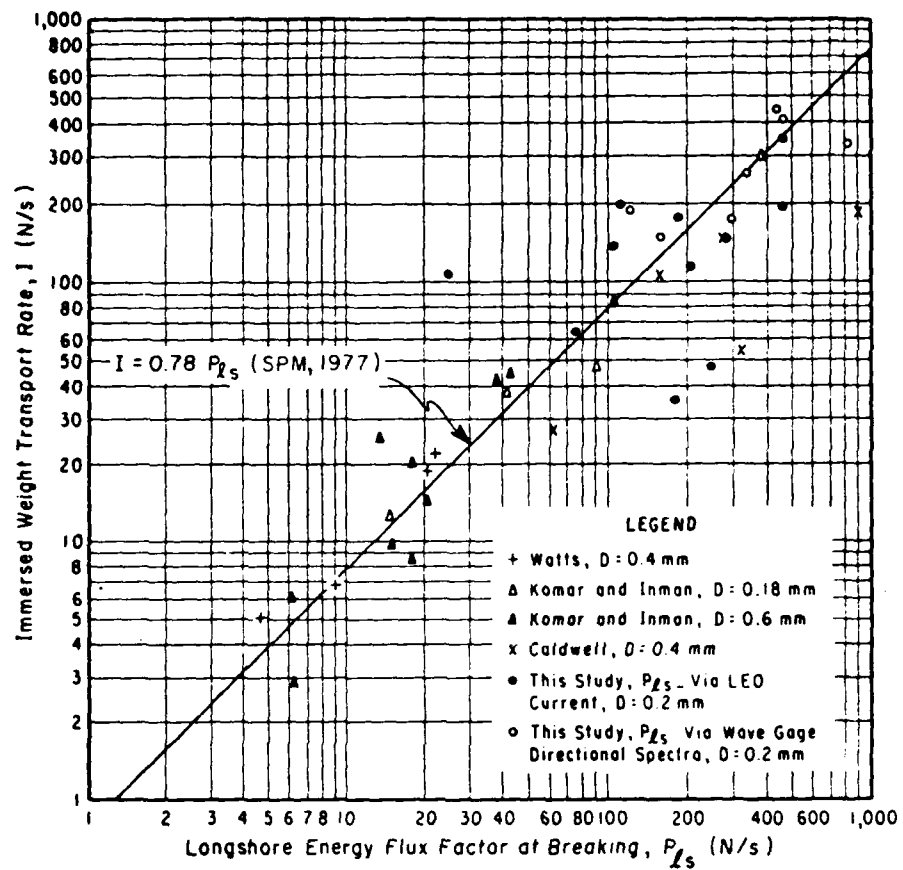


Figure 18. Summary of field data I versus P_{ls} , including results of this study.

Using the data in the SPM sand transport relationship along with the results of the present study, an average \bar{K} can be found, based on 42 field data points, to be $\bar{K} = 0.87$.

This value of \bar{K} is only 11.5 percent higher than the existing value of K in the SPM. In view of the large standard deviations encountered in the data sets, it is suggested that the existing SPM relationship remain unchanged until additional quality data are analyzed in future studies.

5. Conclusions.

Measurements of immersed sediment transport rate, I , as inferred from sediment accumulation in a near-total trap were correlated with longshore energy flux factor at breaking, P_{ls} , as calculated in phase I from two pressure sensors mounted near the bottom and in phase II from LEO wave height and longshore current observations. Based on the analysis of 7 correlation periods between sand accumulation and wave gage data (phase I) 11 correlation periods between sand accumulation and LEO wave observations (phase II), it is concluded that:

(a) On an overall basis, the results of the present study agree reasonably well with some of the previous studies. The dimensionless constant K in the relationship $I = KP_{ls}$ was found to range from 0.19 to 4.18 with an average value $\bar{K} = 0.98$ for the Channel Islands data. In view of the large scatter within the data set, it is recommended that no change be made in the SPM (U.S. Army, Corps of Engineers, Coastal Engineering Research Center, 1977) relationship for sand transport.

(b) For the phase I survey periods, the K values obtained here are substantially lower than those based on visual wave estimates obtained by Bruno and Gable (1976). Their average K value is 1.40 as compared to 0.98 obtained here for the Channel Islands data.

(c) A pair of wave gages appears to perform reasonably well to determine overall directional characteristics such as P_{ls} ; however, the quality of the detailed directional results could be improved substantially by a greater number of gages.

(d) In calculating wave direction from an array of gages, it is extremely important to accurately determine the relative locations of the gages and the shoreline orientation. For the present data, an angular misalignment of $+0.5^\circ$ can cause an associated change in P_{ls} , ranging from 8 to 18 percent.

(e) LEO wave height observations appear to be subjective with strong observer bias. As a result, LEO measurements should be correlated with wave gage or other instrumentation measurements before their acceptance.

(f) There are variations in the K values that cannot be explained through any evident mechanisms or processes other than poor data quality in specific data sets.

(g) The environmental and economic significance of an improved quantitative predictor for longshore sediment transport justifies substantial future field programs to discern the effects of individual variables (e.g., grain size, beach slope, etc.) and in general, to develop a more reliable predictor.

LITERATURE CITED

- BEACH EROSION BOARD, "Coast of California, Carpinteria to Pt. Mugu, Beach Erosion Control Study," H.Doc. 29, 83d Congress, 1st sess., U.S. Army, Corps of Engineers, Washington, D.C., 1953.
- BERG, D.W., "Systematic Collection of Beach Data," *Proceedings of the 11th Conference on Coastal Engineering*, American Society of Civil Engineers, Vol. 1, 1968, pp. 273-297 (also Reprint 4-69, U.S. Army, Corps of Engineers, Coastal Engineering Research Center, Washington, D.C., NTIS 697 533).
- BRUNO, R.O., DEAN, R.G., and GABLE, C.G., "Longshore Transport Evaluations at a Detached Breakwater," *Proceedings of the 17th Conference on Coastal Engineering*, American Society of Civil Engineers, 1980, pp. 1-23.
- BRUNO, R.O., and GABLE, C.G., "Longshore Transport at a Total Littoral Barrier," *Proceedings of the 15th International Conference on Coastal Engineering*, American Society of Civil Engineers, Vol. II, 1976, pp. 1203-1222 (also Reprint 77-6, U.S. Army, Corps of Engineers, Coastal Engineering Research Center, Fort Belvoir, Va., NTIS A042 473).
- BRUNO, R.O., and HIIPAKKA, L.W., "Littoral Environment Observation Program in the State of Michigan," *Proceedings of the 16th Conference on Great Lakes Research*, International Association on Great Lakes Research, 1973, pp. 492-507.
- BRUNO, R.O., WATTS, G.M., and GABLE, C.G., "Sediments Impounded by an Offshore Breakwater," *Proceedings of the Coastal Sediments '77 Specialty Conference*, American Society of Civil Engineers, 1977, pp. 1006-1025 (also Reprint 78-8, U.S. Army, Corps of Engineers, Coastal Engineering Research Center, Fort Belvoir, Va., NTIS A051 577).
- CALDWELL, J.W., "Wave Action and Sand Movement Near Anaheim Bay, California," TM-68, U.S. Army, Corps of Engineers, Beach Erosion Board, Washington, D.C., Feb. 1956.
- DAS, M.M., "Longshore Sediment Transport Rates: A Compilation of Data," MP 1-71, U.S. Army, Corps of Engineers, Coastal Engineering Research Center, Washington, D.C., Sept. 1971.
- DEAN, R.G., "Heuristic Models of Sand Transport in the Surf Zone," *Proceedings of the Conference on Engineering Dynamics in the Surf Zone*, Institution of Engineers, 1973, pp. 208-214.
- GALVIN, C.J., and SCHWEPPE, C.R., "The SPM Energy Flux Method for Predicting Longshore Transport Rate," TP 80-4, U.S. Army, Corps of Engineers, Coastal Engineering Research Center, Fort Belvoir, Va., June 1980.
- GREER, M.N., and MADSEN, O.S., "Longshore Sediment Transport Data: A Review," *Proceedings of the 16th Conference on Coastal Engineering*, American Society of Civil Engineers, Ch. 93, 1978, pp. 1563-1576.
- HARRIS, F.J., "Windows, Harmonic Analysis, and the Discrete Fourier Transform," Report NUC TP-532. U.S. Naval Undersea Center, San Diego, Calif., Sept. 1976.

- HERRON, W.J., and HARRIS, R.L., "Littoral Bypassing and Beach Restoration in the Vicinity of Port Hueneme, California," *Proceedings of the 10th Conference on Coastal Engineering*, American Society of Civil Engineers, Vol. 1, 1966, pp. 651-675.
- KOMAR, P.D., and INMAN, D.L., "Longshore Sand Transport on Beaches," *Journal of Geophysical Research*, Vol. 75, No. 30, Oct. 1970, pp. 5914-5927.
- LONGUET-HIGGINS, M.S., "On the Statistical Distribution of the Heights of Sea Waves," *Journal of Marine Research*, Vol. 11, No. 3, 1967, pp. 245-266.
- LONGUET-HIGGINS, M.S., "Longshore Currents Generated by Obliquely Incident Sea Waves, 1 and 2," *Journal of Geophysical Research*, Vol. 75, No. 33, Nov. 1970, pp. 6778-6801.
- MOORE, G.W., and COLE, J.Y., "Coastal Processes in the Vicinity of Cape Thompson, Alaska; Geologic Investigations in Support of Project Chariot in the Vicinity of Cape Thompson, Northwestern Alaska - Preliminary Report," U.S. Geological Survey Trace Elements Investigations Report 753, 1960.
- SAVAGE, R.P., "Sand Bypassing at Port Hueneme, California," TM-92, U.S. Army, Corps of Engineers, Beach Erosion Board, Washington, D.C., Mar. 1957.
- U.S. ARMY, CORPS OF ENGINEERS, COASTAL ENGINEERING RESEARCH CENTER, *Shore Protection Manual*, 3d ed., Vols. I, II, and III, Stock No. 008-022-00113-1, U.S. Government Printing Office, Washington, D.C., 1977, 1,262 pp.
- U.S. ARMY ENGINEER DISTRICT, LOS ANGELES, "Harbor and Shore Protection in the Vicinity of Port Hueneme, California," Los Angeles, Calif., 1948, pp. 1-71.
- VITALE, P., "A Guide for Estimating Longshore Transport Rate Using Four SPM Methods," CETA 80-6, U.S. Army, Corps of Engineers, Coastal Engineering Research Center, Fort Belvoir, Va., Apr. 1980.
- WALTON, T.L., Jr., "Littoral Sand Transport on Beaches," Ph.D. Dissertation, University of Florida, Gainesville, Fla., 1979.
- WATTS, G.M., "A Study of Sand Movement at South Lake Worth Inlet, Florida," TM-42, U.S. Army, Corps of Engineers, Beach Erosion Board, Washington, D.C., Oct. 1953.

APPENDIX A

DERIVATION OF EQUATION (9) FOR LONGSHORE ENERGY FLUX

a. From Longuet-Higgins (1970)

$$v_b = \frac{5\pi}{16} \left(\frac{\kappa\beta}{C_f} \right) (gd_b)^{1/2} (m \sin \alpha_b \cos \alpha_b) \quad (A-1)$$

where

β = a mixing parameter (dimensionless)

d_b = breaking depth

m = beach slope

α_b = breaking wave angle

b. Using relationship

$$\kappa = \frac{H_b}{d_b} \quad (A-2)$$

equation (A-1) becomes

$$v_b = \frac{5\pi}{32} \left(\frac{\kappa\beta}{C_f} \right) \frac{1}{\sqrt{\kappa}} (\sqrt{gH_b} m \sin 2\alpha_b) \quad (A-3)$$

c. Longshore velocity at any point within the surf zone can be defined as

$$v = v_b \left(\frac{V_o}{V_b} \right) \left(\frac{V}{V_o} \right) \quad (A-4)$$

where V is the longshore current within surf zone and V_o the theoretical longshore velocity at breaking with no mixing.

d. From equation (58) in Longuet-Higgins (1970)

$$\frac{V_o}{V_b} = \frac{1}{\beta} \quad (A-5)$$

e. Using equations (A-3), (A-4), and (A-5), longshore velocity is

$$v = \left(\frac{V}{V_o} \right) \left(\frac{5\pi}{32} \right) \left(\frac{\kappa}{C_f} \right) \left(\frac{1}{\sqrt{\kappa}} \right) (m \sqrt{gH_b} \sin 2\alpha_b) \quad (A-6)$$

f. Using equation (4-40) in the SPM

$$P_{\ell s} = \frac{\rho g H_b^2}{16} C \sin 2\alpha_b \quad (A-7)$$

where $C = \text{group celerity} = \sqrt{gd_b}$ according to linear shallow-water wave theory; therefore,

$$P_{\ell s} = \frac{\rho g H_b^2}{16} \left(\frac{d_b}{H_b} \right)^{1/2} \sqrt{gH_b} \sin 2\alpha_b \quad (A-8)$$

g. Using equations (A-2), (A-6), and (A-8), and assuming $m = W/d_b$, the following equation is found:

$$P_{\ell s} = \frac{\rho g H_b W V C_f}{\left(\frac{5\pi}{2}\right) \left(\frac{V}{V_o}\right)} \quad (A-9)$$

h. The value of (V/V_o) can be assumed equal to that given by Longuet-Higgins (1970)

$$\frac{V}{V_o} = \left(\frac{V}{V_o}\right)_{LH} \quad (A-10)$$

i. Equation (A-9) now becomes

$$P_{\ell s} = \frac{\rho g H_b W V C_f}{\left(\frac{5\pi}{2}\right) \left(\frac{V}{V_o}\right)_{LH}} \quad (A-11)$$

APPENDIX B
CALCULATIONS OF LONGSHORE ENERGY FLUX FACTORS

Table B-1. Net longshore energy flux factors calculated by use of LEO current data and LEO wave angle data
 (based on Hrms values).¹

Comparative survey	Dates	Obsns.	LEO station 5715 (north)			LEO station 5714 (middle)			LEO station 5713 (south)		
			R ²	P _{Ls} (eq. 7) (N/s)	P _{Ls} (eq. 9) (N/s)	R ²	P _{Ls} (eq. 7) (N/s)	P _{Ls} (eq. 9) (N/s)	R ²	P _{Ls} (eq. 7) (N/s)	P _{Ls} (eq. 9) (N/s)
Phase I											
1	17 Apr. to 7 May 1974	42	0.10	-202.48	-517.09	0.04	-189.57	-511.31	-0.03	-195.80	-410.29
2	7 May to 30 July 1974	168	0.62	-88.11	-199.36	0.61	-88.11	-227.84	0.52	-135.73	-232.29
3	30 July to 20 Aug. 1974	40	0.64	-29.37	21.23	0.55	-24.92	-81.44	0.08	-40.41	-39.20
4	20 Aug. to 24 Sept. 1974	68	0.66	-22.74	-19.71	0.74	-19.36	-15.35	0.27	-53.40	-48.95
5	24 Sept. to 6 Nov. 1974	84	0.60	-34.75	-96.57	0.74	-38.40	-122.82	0.59	-59.19	-125.94
6	6 Nov. 1974 to 7 Jan. 1975	115	0.38	-55.18	-141.07	0.21	-56.52	-184.23	0.14	-66.31	-97.01
7	7 Jan to 11 Feb. 1975	69	0.35	-73.87	-230.96	0.34	-93.90	-246.53	-0.07	-96.12	-129.50
8	11 Feb. to 4 Mar. 1975	41	0.54	-61.41	-176.22	0.37	-53.85	-157.98	0.13	-60.52	-94.79
9	4 Mar. to 14 Apr. 1975	78	0.26	-46.73	-284.36	0.33	-49.40	-230.51	0.16	-68.09	-101.02
10	14 Apr. to 6 May 1975	37	0.03	-45.84	-207.82	0.41	-44.95	-185.12	0.04	-57.85	-161.54
11	6 May to 1 Aug. 1975	168	0.48	-16.24	-52.07	0.52	-16.78	-41.21	0.20	-23.50	-48.51
12	1 Aug. to 13 Aug. 1975	24	0.52	-14.20	-18.11	0.65	-16.73	-39.69	0.08	-31.64	0.76
13	13 Aug. to 16 Sept. 1975	68	0.70	-12.59	11.66	0.65	12.50	9.79	-0.19	-9.52	-8.10
Phase II											
14	28 Jan. to 20 Apr. 1976	164	0.27	-94.30	-486.39	0.24	-97.90	-392.05	0.06	-91.67	-364.90
15	20 Apr. to 20 May 1976	59	0.29	-49.84	-188.68	0.24	-44.01	-206.48	-0.18	-44.95	-132.61
16	20 May to 28 June 1976	75	0.38	-29.64	-105.91	0.40	-31.33	-112.59	-0.13	-35.60	-126.83
17	28 June to 12 Aug. 1976	86	0.53	-2.98	-72.09	0.37	13.48	-91.67	0.22	-28.44	-82.77
18	12 Aug to 8 Sept. 1976	50	0.49	11.53	25.85	0.41	11.88	22.34	0.43	-14.95	3.03
19	8 Sept. to 6 Oct. 1976	55	0.51	-51.18	-213.60	0.32	-40.23	-72.54	0.32	-40.67	-29.59
20	6 Oct. to 1 Dec. 1976	106	0.16	-107.25	-224.37	0.20	-102.78	-260.33	0.26	-69.42	-109.03
21	1 Dec. 1976 to 3 Feb. 1977	125	0.39	-95.23	-252.32	0.41	-79.66	-238.97	0.17	-49.84	-160.20
22	3 Feb. to 22 Mar. 1977	89	0.51	-125.05	-460.55	0.41	-114.81	-445.45	0.13	-72.09	-213.16
23	22 Mar. to 27 Apr. 1977	67	0.43	-101.02	-336.68	0.45	-102.35	-456.13	0.24	-56.96	-258.10
24	27 Apr. to 6 June 1977	78	0.47	-82.33	-449.45	0.52	-76.99	-540.23	0.30	-52.51	-345.77
25	6 June to 21 July 1977	85	0.76	12.91	0.13	0.70	30.71	69.42	0.48	-28.93	-49.40
26	21 July to 30 Aug. 1977	78	0.65	-48.51	-145.52	0.65	-42.76	-161.09	0.35	-32.31	-24.34

¹Negative values of longshore energy flux factor signify flux toward the trap.

²R = correlation coefficient between observed longshore current and theoretical (Longuet-Higgins, 1970) longshore current.

Table B-2. Negative longshore energy flux factors calculated by use of LEO current data and LEO wave angle data (based on Hrms values).¹

Comparative survey	Dates	Obsns.	LEO station 5715 (north)			LEO station 5714 (middle)		
			R ²	P _{Ls} (eq. 7) (N/s)	P _{Ls} (eq. 9) (N/s)	R ²	P _{Ls} (eq. 7) (N/s)	P _{Ls} (eq. 9) (N/s)
Phase I								
1	17 Apr. to 7 May 1974	42	0.10	-202.92	-531.78	0.04	-189.57	-405.40
2	7 May to 30 July 1974	168	0.62	-97.46	-217.61	0.61	-98.79	-208.71
3	30 July to 20 Aug. 1974	40	0.64	-36.49	-90.34	0.55	-38.27	-117.04
4	20 Aug. to 24 Sept. 1974	68	0.66	-28.48	-29.82	0.74	-33.82	-113.48
5	24 Sept. to 6 Nov. 1974	84	0.60	-45.84	-121.04	0.74	-50.29	-23.14
6	6 Nov. 1974 to 7 Jan. 1975	115	0.38	-56.96	-171.77	0.21	-57.41	-117.04
7	7 Jan. to 11 Feb. 1975	69	0.35	-74.76	-230.96	0.34	-94.34	-267.89
8	11 Feb. to 4 Mar. 1975	41	0.54	-62.75	-176.22	0.37	-54.74	-267.89
9	4 Mar. to 14 Apr. 1975	78	0.26	-54.29	-311.06	0.33	-59.63	-460.58
10	14 Apr. to 6 May 1975	37	0.03	-47.62	-208.26	0.41	-47.62	-472.15
11	6 May to 1 Aug. 1975	168	0.48	-21.36	-77.88	0.52	-23.14	-544.68
12	1 Aug. to 13 Aug. 1975	24	0.52	-20.92	-30.71	0.65	-24.03	-61.86
13	13 Aug. to 16 Sept. 1975	68	0.70	-4.45	-22.70	0.65	-4.01	-189.13
Phase II								
14	28 Jan. to 20 Apr. 1976	164	0.27	-101.91	-499.74	0.24	-101.02	-516.65
15	20 Apr. to 20 May 1976	59	0.29	-50.29	-199.36	0.24	-45.39	-255.43
16	20 May to 28 June 1976	75	0.38	-33.38	-112.59	0.40	-33.82	-101.46
17	28 June to 12 Aug. 1976	86	0.53	-37.38	-103.69	0.37	-38.27	-36.49
18	12 Aug. to 8 Sept. 1976	50	0.49	-16.02	-28.04	0.41	-14.69	-142.85
19	8 Sept. to 6 Oct. 1976	55	0.51	-83.66	-258.55	0.32	-68.09	-186.01
20	6 Oct. to 1 Dec. 1976	106	0.16	-109.47	-232.74	0.20	-104.58	-246.53
21	1 Dec. 1976 to 3 Feb. 1977	125	0.39	-102.80	-291.03	0.41	-85.44	-157.98
22	3 Feb. to 22 Mar. 1977	89	0.51	-127.27	-478.38	0.41	-118.37	-305.72
23	22 Mar. to 27 Apr. 1977	67	0.43	-101.02	-370.24	0.45	-103.24	-190.46
24	27 Apr. to 6 June 1977	78	0.47	-91.67	-460.58	0.52	-89.00	-74.32
25	6 June to 21 July 1977	85	0.76	-31.60	-94.79	0.70	-29.37	-52.51
26	21 July to 30 Aug. 1977	78	0.65	-58.74	-179.34	0.65	-55.63	-18.25

¹Negative values of longshore energy flux factor signify flux toward the trap.

²R = correlation coefficient between observed longshore current and theoretical (Longuet-Higgins, 1970) longshore current.

Table B-3. Ratio of cumulative longshore energy fluxes using LEO data.

Comparative survey	Dates	Obsns.	Ratio= $\Sigma P_{ls^+}/\Sigma P_{ls^-}$
Phase I			
1	17 Apr. to 7 May 1974	42	0.030
2	7 May to 30 July 1974	168	0.084
3	30 July to 20 Aug. 1974	40	1.234
4	20 Aug. to 24 Sept. 1974	68	0.334
5	24 Sept. to 6 Nov. 1974	84	0.204
6	6 Nov. 1974 to 7 Jan. 1975	115	0.179
7	7 Jan. to 11 Feb. 1975	69	0.000
8	11 Feb. to 4 Mar. 1975	41	0.000
9	4 Mar. to 14 Apr. 1975	78	0.086
10	14 Apr. to 6 May 1975	37	0.003
11	6 May to 1 Aug. 1975	168	0.332
12	1 Aug. to 13 Aug. 1975	24	0.410
13	13 Aug. to 16 Sept. 1975	68	1.520
Phase II			
14	28 Jan. to 20 Apr. 1976	164	0.027
15	20 Apr. to 20 May 1976	59	0.054
16	20 May to 28 June 1976	75	0.061
17	28 June to 12 Aug. 1976	86	0.305
18	12 Aug. to 8 Sept. 1976	50	1.923
19	8 Sept. to 6 Oct. 1976	55	0.174
20	6 Oct. to 1 Dec. 1976	106	0.035
21	1 Dec. 1976 to 3 Feb. 1977	125	0.132
22	3 Feb. to 22 Mar. 1977	89	0.080
23	22 Mar. to 27 Apr. 1977	67	0.021
24	27 Apr. to 6 June 1977	78	0.016
25	6 June to 21 July 1977	85	1.001
26	21 July to 30 Aug. 1977	78	0.189

Note.--Positive longshore energy flux factor signifies energy flux to the north (right when looking offshore); negative longshore energy flux factor signifies energy flux to the south (left when looking offshore).

